



# Extrusion-Based Technology in Additive Manufacturing: A Comprehensive Review

Abhishek Patel<sup>1</sup> · Mohammad Taufik<sup>1</sup>

Received: 17 June 2022 / Accepted: 12 December 2022 / Published online: 27 December 2022  
© King Fahd University of Petroleum & Minerals 2022

## Abstract

Extrusion-based additive manufacturing (EB-AM) is a 3D fabrication process in which the material is heated and extracted through a nozzle before being deposited one layer at a time. It uses two types of technologies: filament and pellet extrusion. Filament extrusion machines entail transforming raw plastic pellets into a spool of filament; hence, these machines use limited materials. Pellet extrusion printers are more complex machines and use a screw inside a barrel. Screw feeds, transports, and melts the material before forcing it to be deposited at the required temperatures. Besides the complexities, a pellet extruder offers lower costs, higher speeds, and a wide variety of materials that can be used. This paper presents the development in extrusion-based 3D printing addressing filament and pellet-based printing issues, including filament breakage, nozzle clogging, in-line rheological monitoring, multi-color printing, material retraction, and cost-effectiveness of pellet-based extrusion additive manufacturing. To improve the material domain for 3D printing and utilize the advantages of filament and pellet-based extrusion, a hybrid form of 3D printer can be developed, capable of printing both filaments and pellet forms of material. This review work is intended to help young researchers in the field of EB-AM to understand the advances of this technology and its related complexities.

**Keywords** Additive manufacturing · Extrusion-based 3D printing · Filament extruder · Pellet extruder

## Abbreviations

EB-AM	Extrusion-based additive manufacturing
AM	Additive manufacturing
ALM	Additive layer manufacturing
DMLS	Direct metal laser sintering
DMLM	Direct metal laser melting
SLS	Selective laser sintering
SHS	Selective heat sintering
EBM	Electron beam melting
LOM	Laminated object manufacturing
UAM	Ultrasonic additive manufacturing
UV	Ultraviolet
CAD	Computer-aided design
STL	Standard tessellation language
FFF	Fused filament fabrication

FDM	Fused deposition modeling
SFF	Solid freeform fabrication
PTFE	Polytetrafluoroethylene
PC	Polycarbonate
HIPS	High-impact polystyrene
DAQ	Data acquisition device
AE	Acoustic emission
BMGs	Bulk metallic glasses
PLA	Polylactic acid
ABS	Acrylonitrile butadiene styrene
PLA	Polylactic acid
PS	Polystyrene
HIPS	High impact polystyrene
PETG	Polyethylene terephthalate glycol
PBT	Polybutylene terephthalate
PBS	Polybutylene succinate
PMMA	Poly-methyl methacrylate
HDPE	High-density polyethylene
TPU	Thermoplastic polyurethane
PEI	Poly ethylenimine
PEEK	Polyether ether ketone
PPSF	Poly phenyl sulfone

✉ Mohammad Taufik  
mohammad.taufik@manit.ac.in

<sup>1</sup> Department of Mechanical Engineering, Maulana Azad National Institute of Technology (MANIT), Bhopal 462003, India



PEKK	Poly ether ketone ketone
PP	Polypropylene
PVC	Polyvinyl chloride
IFBS	Interfacial bond strength
MCE	Microchip capillary electrophoresis
C <sup>4</sup> D	Capacitively coupled contactless conductivity detection
BGE	Background electrolyte

## 1 Introduction

3D printing, commonly referred to as additive layer manufacturing (ALM) or additive manufacturing (AM), is a computer-aided production technology for creating three-dimensional objects by material fabrication. Additive manufacturing enables the production of custom parts for complicated geometries with minimal waste. The computerized process is handy for rapid prototyping as the changes in design can be done quickly and effectively, even at the time of manufacturing. The minimal wastage of materials reduces costs for high-value objects [1]; lead times have also been reduced. Furthermore, components that formerly mandated numerous components to be assembled can be made as a cohesive unit, leading to increased durability and strength. Some AM technologies even have the advantage of processing multiple materials [2]. Additive manufacturing can generate one-of-a-kind components or replacements for no longer manufactured parts. This technology is used to manufacture a wide variety of objects in many sectors because of its weight-saving capacity to make complicated geometric pieces. 3D printing provides an opportunity to improve the part quality at all stages of manufacturing, pre-processing, on-situ, and post-processing stages [3]. Components can be fabricated quickly and also results in the reduction of cost, in aerospace, and defense [4, 5], the automotive industry [6], the medical industry, particularly for custom-fitted implants and devices [7], fashion, and jewelry [8].

There are various AM methods, each with its specification. The AM method includes; binder jetting, which consists of depositing alternate layers of material powder and binder in liquid form, which acts as an adhesive by moving a 3D printer head along the *x*, *y*, and *z* axes. In the directed energy deposition process, the material is melted using a concentrated source of energy such as an electron beam, plasma, or laser, and the nozzle deposits it on a vertically moving bed. Coiled materials are either dispensed or pulled through a heated nozzle positioned on a moving arm in material extrusion. As the nozzle travels horizontally and the platform moves vertically, melted material is deposited layer after layer. Powder bed fusion involves melting or partially melting thin material layers using a beam of electrons, laser beam, or high-temperature print heads, followed by blasting away

extraneous powder [9]. Direct metal laser sintering (DMLS), direct metal laser melting (DMLM), selective laser sintering (SLS), selective heat sintering (SHS), and electron beam melting (EBM) all of these are cases of powder bed fusion processes. Sheet lamination is an AM process that involves laminating thin sheets of material together layer by layer to create a single part. Sheet lamination can be categorized into two principal methodologies; laminated object manufacturing (LOM) and ultrasonic additive manufacturing (UAM). LOM uses alternating layers of paper and adhesive to produce visually and aesthetically pleasing products. UAM utilizes ultrasonic welding to fabricate thin sheets of numerous metals, including aluminum, stainless steel, and titanium, at low temperatures and low energy. Vat polymerization employs a vat of liquid resin photopolymer to build a part layer upon layer. Ultraviolet (UV) light is focused by employing mirrors to cure each resin layer by photopolymerization.

Although the additive manufacturing process flow varies depending on which additive manufacturing process is used to build the 3D components, they all follow the same basic processes to make the final product, as shown in diagram 1. The first step is to create a 3D image of the product utilizing computer-aided design (CAD) software or a 3D object scanner; a 3D image is first generated. The second step requires converting the generated 3D image to a standard tessellation language (STL) file to tessellate the 3D image, and slicing is done to split the 3D image into multiple layers [10]. The next step is to the STL file to a printer using a specialized machine program. Resources are allocated, and the machine is set up with the printing parameters. Once the machine is set with printing parameters, an actual model is constructed layer after layer by depositing material. The next step is part removal, in which the model is detached from the build platform and its supporting framework. Finally, post-processing may be required for value addition, such as cleaning, plating, coating, laser polishing, local surface heating, and annealing [11] (Fig. 1).

Since this research work aims to review the filament and screw-assisted EB-AM processes, the instructions provided by Siddaway et al. were used to create a review methodology [12]. Science Direct, Web of Science, and Scopus were the three electronic datasets utilized, with keywords additive manufacturing, 3D printing, material extrusion, pellet-based extruder, multi-material printing, and big area additive manufacturing. Only publications designated as research articles were taken into consideration for the assessment, which spanned the years 2000–2022. All shortlisted research was assessed by reading the title of the article, abstract, and keywords and duplicate articles were eliminated, considering only the most recent research. Assessment criteria include: (a) material extrusion should be the foundation of the process of 3D printing, and (b) 3D printers should receive material directly, either in filament or pellet form.

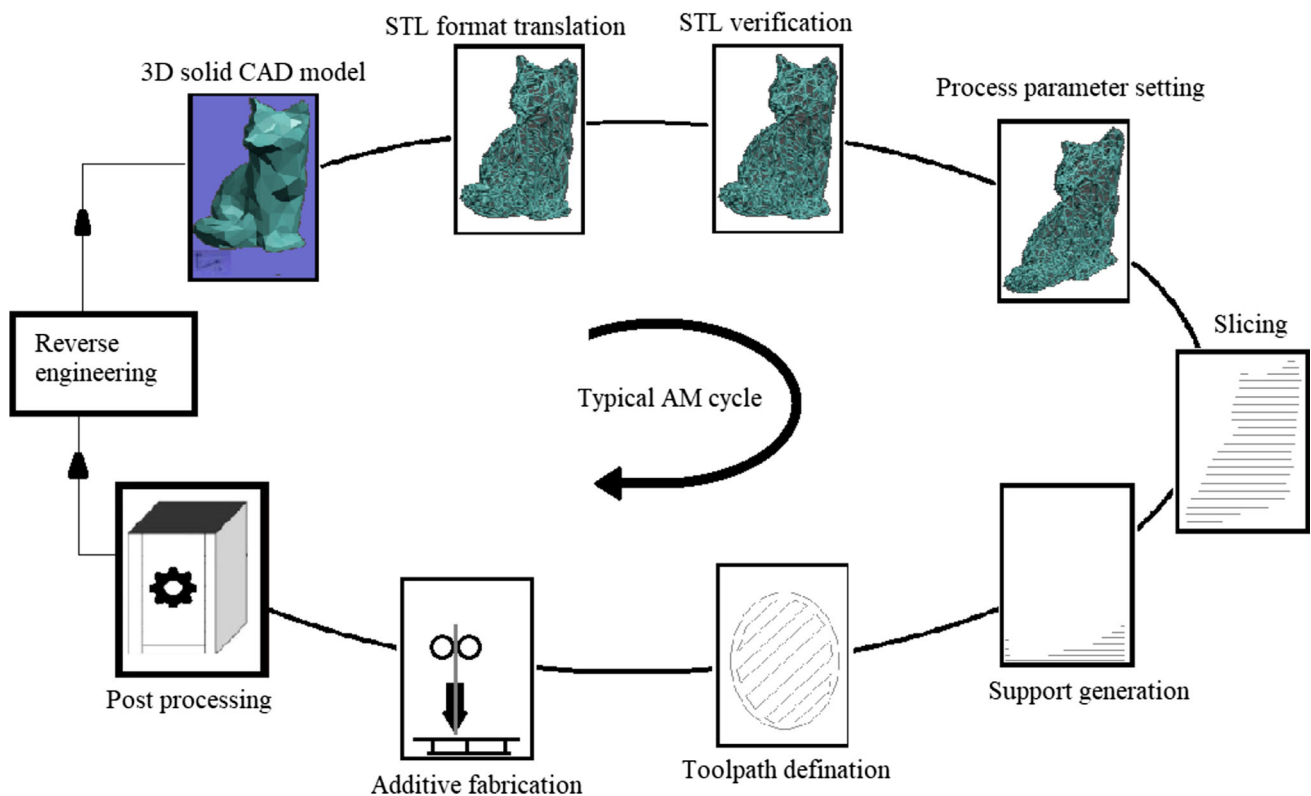


Fig. 1 Additive manufacturing cycle

To ensure that only the working apparatus that may have been used for processing/deposition tests were taken into consideration, the pre-selected papers were carefully examined to more thoroughly research their impact on the fields of multi-material printing and extrusion-based additive manufacturing. Lastly, the publications were reviewed about: (i) the type of extrusion-based AM (i.e., filament-based or pellet-based), (ii) scale of manufacturing (i.e., large volume or small volume), and (iii) the primary adjustments made to the printing units in consideration of multi-material printing.

As this paper presents a review of EB-AM processes, this section begins with extrusion-based rapid prototyping. Extrusion-based rapid prototyping, such as fused filament fabrication (FFF), or fused deposition modeling (FDM), is gaining popularity in academics and industry. Because it uses economic technology and enduring part materials, EB-AM is among the most extensively utilized solid freeform fabrication (SFF) technologies [13]. While EB-AM works the same way as other 3D printing methods in that layer after layer is created, it differs as the material is continuously supplied and deposited via a nozzle at constant pressure. EB-AM is a 3D printing process that uses a constant flow of thermoplastic polymers or their composites to create 3D objects. The schematic of EB-AM is illustrated in Fig. 2. Thermoplastic or composite material is fed to an extruding nozzle; inside

the nozzle, the material is heated and extruded out to deposit on the build platform layer after layer.

Extrusion-based 3D printers use either Bowden extruder or direct drive extruder setups. The working principle of both extruders is the same only difference lies in where the extruder is placed (Fig. 3). The extruder is commonly installed on the printer’s frame in a Bowden arrangement. As a result, the filament goes to the hot end via a polytetrafluoroethylene (PTFE) tube. Bowden tube arrangement offers the advantage of cleaner movement as significantly less weight is on the carriage; hence, movements are quicker and quieter, and print quality is high. In this configuration extruder has to push the filament through a long tube; hence high motor power is required, response time is low, and it involves materials complications as some materials can wear the Bowden tube. Meanwhile, the extruder is positioned on the printhead in a direct drive arrangement, pushing the filament straight into the hot end. A direct extrusion system offers the advantages of reliable extrusion, better retraction, a less powerful motor, and a wide range of filament materials. This system has vibrations and cumbersome maintenance because of added weight on the printhead. Extra weight reduces speed, increases wobble and likely loses X and Y movement accuracy.

EB-AM can produce parts of controlled properties: porosity, density, or mechanical properties. As technology grows,

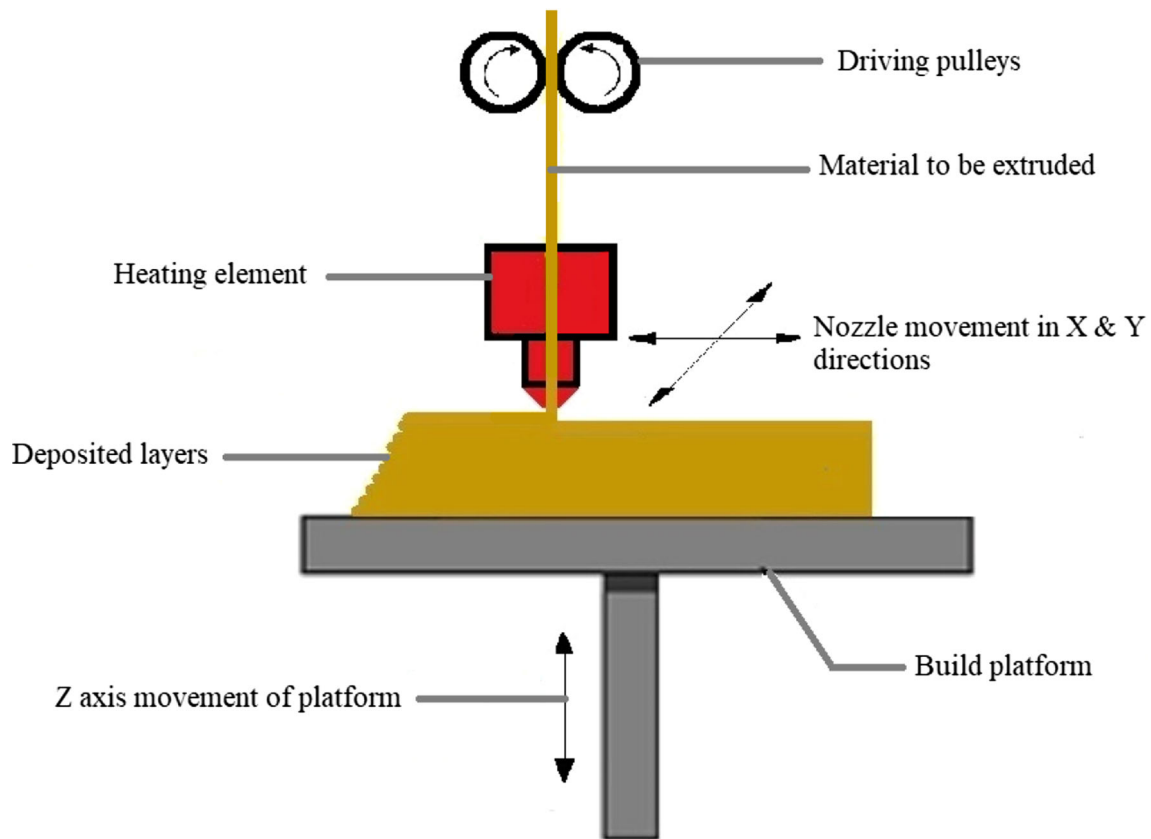


Fig. 2 Schematic of material extrusion additive manufacturing

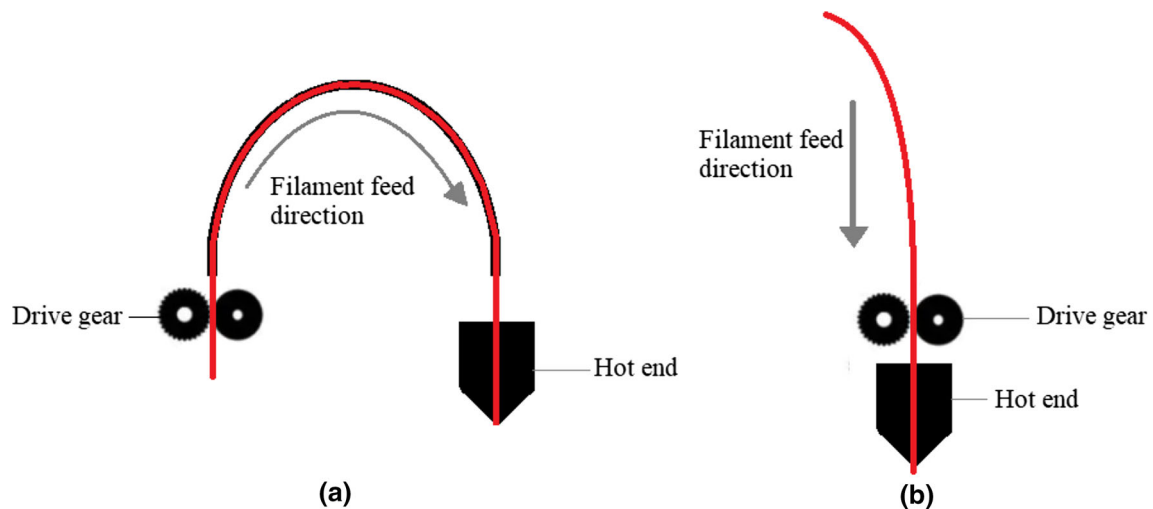
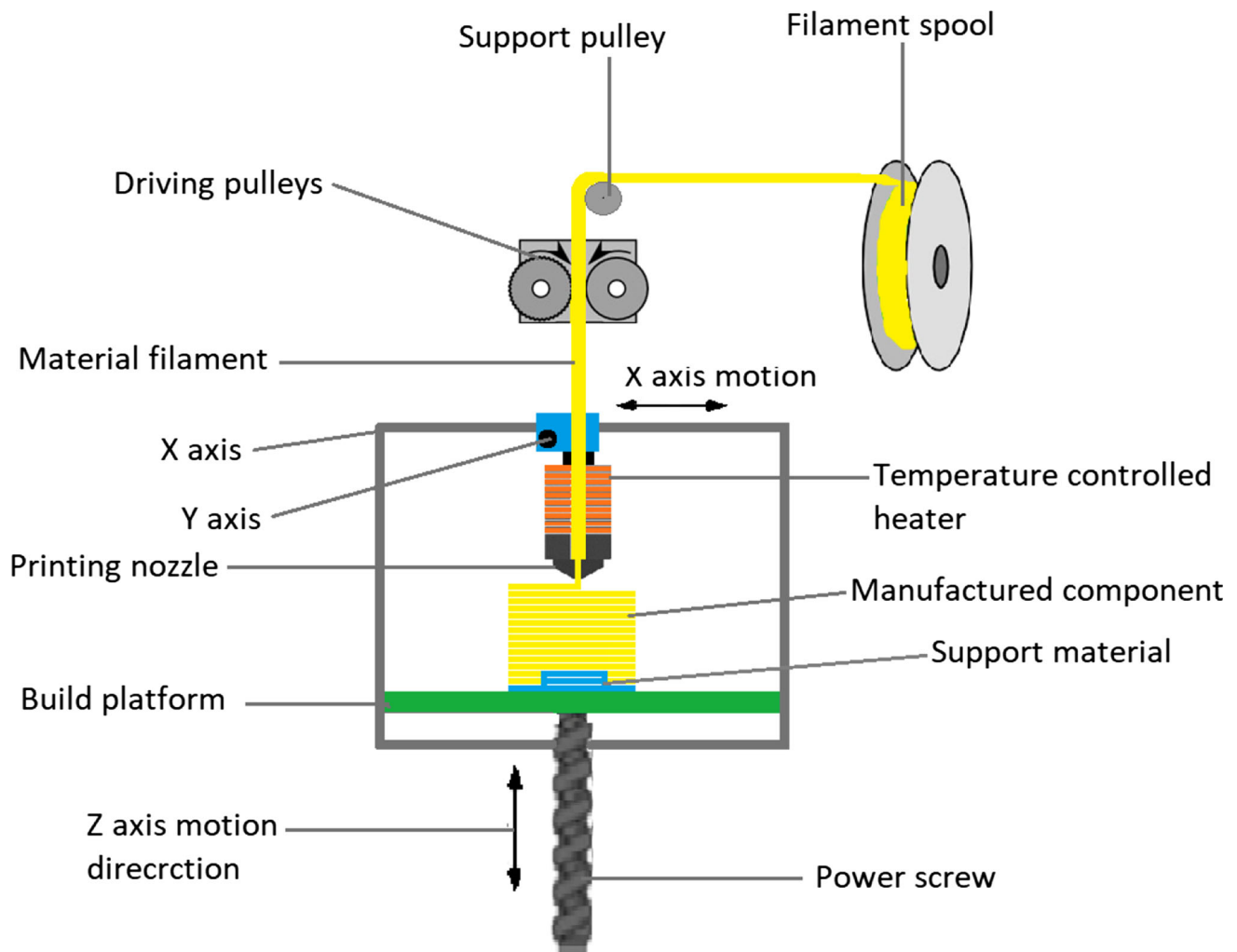


Fig. 3 Extruder systems: **a** Bowden configuration; **b** direct configuration

manufacturing functional parts and prototypes are becoming possible. Still, specific improvements are required to develop this technology, from prototyping to part manufacturing.

- For parts to maintain their integrity during service, mechanical properties need to be enhanced.
- Need to overcome the limitation of material available for extrusion-based 3D printing.
- Precise control over process parameters to produce dimensionally correct parts with close tolerances.
- Functional parts should have smooth surfaces.



**Fig. 4** Schematic of filament-based extrusion AM

Extrusion-based additive manufacturing is of two types: filament-based and pellet-based manufacturing. The material in the form of filament is continuously supplied in the filament-based process. A filament-based extrusion 3D printer, as shown in Fig. 4, is computer controlled and has a minimum of two extruders: one for base material and one for supporting material. In this machine, parts are manufactured by depositing material in a layered fashion on a platform to give it a prescribed shape as controlled by the computer. When the material is stocked up, it cools, cements, and bonds with the neighbor material. After depositing a layer, the platform moves down by a certain distance, the height of the filament. The next layer is deposited over the already deposited layer. This technology requires minimum human resources and is an advantageous manufacturing method during COVID-like situations where virus spreading is directly proportional to human resources employed. Filament-based 3D printing can manufacture various customized engineering products and find their application in the medical field.

Numerous advancements have been made in developing filament-based 3D printing machines, including process parameters optimization and the development of composite materials [14, 15]. Still, some limitations are needed to be overcome. The low feed rate of the filament extruder is restricted by the diameter of the nozzle aperture and the speed with which the geared wheels drive the filament. The nozzle diameter should be narrower than the filament diameter to sustain the pressure and melt consistency required for good printing, because of which low material deposition rates are obtained. Restricted material choice, the range of filaments available on the market is still steadily increasing, but several plastics containing a high percentage of carbon fiber are too brittle to reel appropriately. The cost of printing with a filament-based extruder is high as it requires an additional cost of preparing filament. Printing significant parts (say 30 kg) is tedious with this method as material spools such large are not feasible, and printing may require 7–8 changes of the

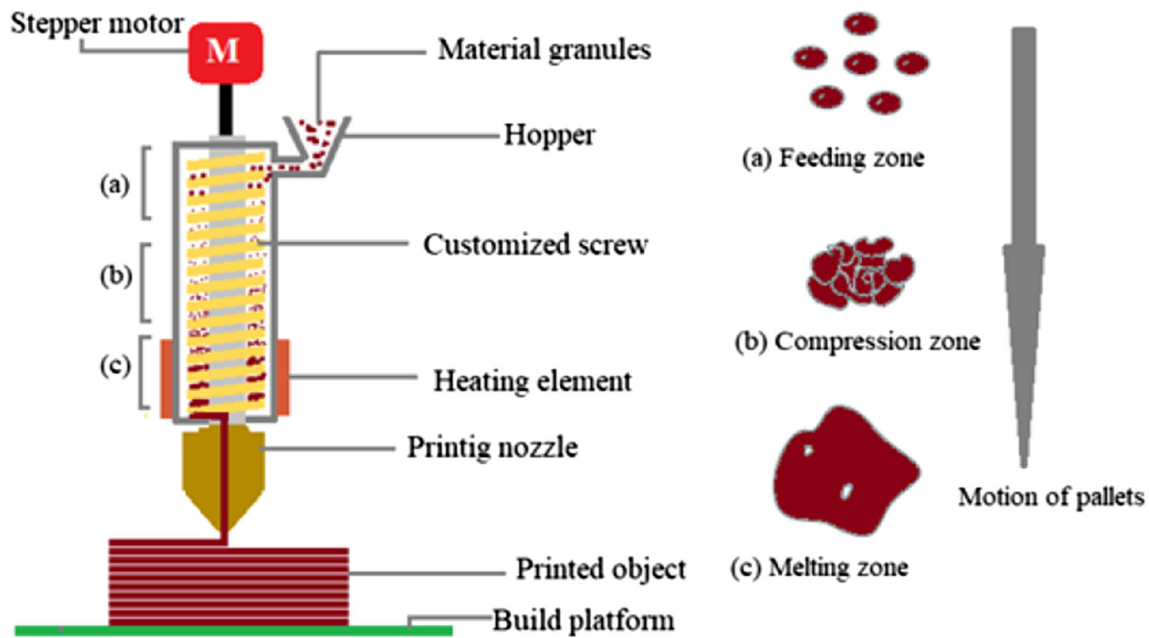


Fig. 5 Schematic of pellet-based extrusion AM

spool. This involves additional problems such as maintaining good layer adhesion since halting the print can result in the additional cooling potential risk of losing heat from its heated chamber during filament change over; this frequently results in distortion/warpage of print. Secondly, a filament-based printing machine is limited to the print filament of one color only at a time, and much time is required to change the filament of different colors.

In pellet-based extrusion 3D printing, as depicted in Fig. 5, material pellets are introduced into a barrel using a hopper, often containing numerous heat zones. A motor-driven screw inside the barrel propels the granules to be discharged through a printing nozzle [16]. There are three zones on the extruder screw: the feeding zone, compression zone, and melting zone (Fig. 5). The molten material is subjected to high pressure before dispensing through a nozzle. The pellet-based system has a lower printing cost as it does not require material in filament form. Two significant factors reduce printing costs; lower material costs and shorter printing times. Nowadays, the industry is shifting toward pellet-based extrusion 3D printers, especially for high carbon fiber materials, which are frequently used to minimize warpage and boost strength. Still, some shortcomings are needed to be overcome for the successful implementation of this method. Inability to couple-up with oozing could result in unpleasant start/stop seams. Pellet extruders typically have various heat zones and varied suggested screw speeds for different materials, making fine-tuning different materials more difficult. It is found that when the larger pellet nozzles are employed for printing, the ejected bead holds quite enough heat and therefore does

not cool down and solidify completely to sustain the next layer; this leads to sagging and printing failure.

Pellet extruders at lower cost offer up many possibilities for 3D printing, and they can usually accelerate a print by a considerable length of time. On the other side, a filament extruder can generate prints with more acceptable tolerances and more complicated shapes.

With the developments in material chemistry and polymer synthesis, new polymer materials are now constantly created and validated for processability and AM suitability. Nowadays high temperature polymer printing is gaining more popularity due to its applications in different fields such as consumer products, biomedical, aerospace, automotive, and high-stress applications. These materials are highly useful as they are applicable in different environmental sectors where heat resistance plays a critical role instead of these materials other materials may melt or soften in these environmental conditions. As shown in Fig. 6, they are divided into three categories depending on physical characteristics and working temperatures: standard plastics, engineering plastics, and advanced ones. Comparing thermoplastic polymer with an aliphatic backbone with high-temperature engineering thermoplastic polymers often containing an aromatic backbone increases the molecular stiffness and decreases the polymer chain mobility. As a result, the processing of engineering thermoplastic polymers usually requires greater temperatures at similar molecular weight ranges. Synthesis and fabrication of high-temperature engineering polymers have been successfully carried out to improve FFF printed parts' performance [17–21].



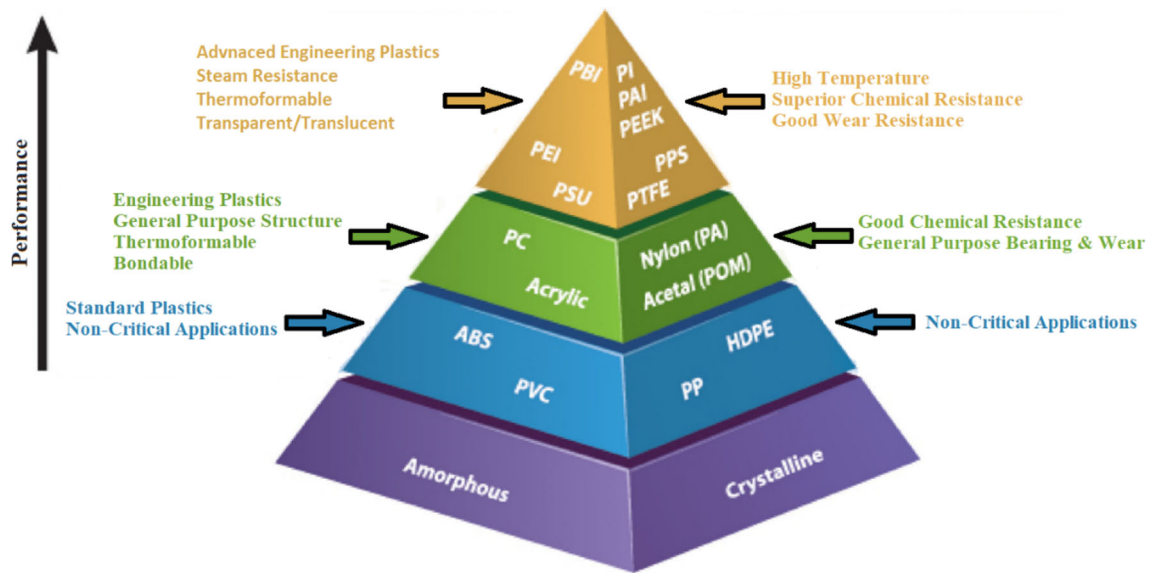


Fig. 6 A summary of high-temperature thermoplastic polymers in terms of performance [22]

Table 1 List of high-temperature polymer printing materials

Name	Properties
Polyether ether ketone (PEEK) [23–25]	Robustness
Polyaryletherketone (PAEK) [26]	Less toxic emissions
Polyvinylidene fluoride (PVDF)	Non-reactive to other materials
Thermoplastic polyimide (TPI) [27]	Abrasion resistance, high-temperature resistance, and long-term durability
Polyetherketoneketone (PEKK)	Compressive force, heat resistance
Polyetherimide (PEI) [28]	Thermal resistance and strength
Polyphenylsulfone (PPSU/ PPSF) [29]	High strength and chemical resistance
Polycarbonate (PC) [30]	great durability, high impact, and scratch resistance

Most of the filament and pellet-operated printers are using low-temperature thermoplastics namely ABS, PLA, and a similar subset of materials. Moreover, with the advances in solid-based part fabrication machine systems can handle a wide variety of materials as they can provide high-temperature nozzle/extruders and build chambers/platforms. A list of high-temperature polymer printing materials along with their properties is given in Table 1.

Apart from the development of high-temperature polymer printing materials, composite filaments and pellets are also developed by mixing different substances along with polymeric materials. In this direction addition of glass, carbon

fiber segments, and similar composite additives are added and utilized to gain the advantage over polymer alone. However, sometimes these additions provide useful results and sometimes offer unexpected properties in composites. Although the bright future of FFF is made possible by its broad range of appropriate polymer and composite materials, especially nanocomposites [31], FFF has significant flaws that have limited its industrial application. FFF printing typically has lower mechanical capabilities than equivalents created using traditional manufacturing techniques and polymer processing, including injection molding. However, mechanical properties can be improved to a certain extent by controlling process parameters and with process modifications [32–34]. The mechanical properties of some typical materials used in FFF are listed in Table 2. Once the melt has left the print head, the pressures are uncontrolled, and the temperature decreases rapidly. As a result, sufficient bonding between the strands is not ensured [35]. In addition to interfacial adhesion, it is essential to consider the impact of voids or porosity on the mechanical characteristics of FFF-printed parts. The existence of voids could interfere with interlayer thermal transmission, weaken the interfacial bonding, and possibly lead to the formation of more voids. Stress concentrations at pores or voids generally lower component performance [36, 37]. Melts undergo shear and extension during the printing process due to nozzle motion, and elliptical cylinders are formed from the elongated melt flow. The strength, stiffness, and porosity of parts produced [38–41] are negatively impacted by pores that develop in-between deposited strands [42–44]. Stage-dependent pre-processing, in situ processing, and post-processing modification in the FFF process can be

**Table 2** Polymer matrix assessment for FFF printing [45]

Polymer	Extrudability	Printability	Mechanical properties	Printing temperature (°C)	UTS (MPa)
PLA	+/-	++	-	190–210	37–46
ABS	++	++	+	210–250	22–37
Nylon	+	+/-	+	235–260	34–68
PS/HIPS	++	+	+/-	240	20–42
PETG	+	++	+/-	230–250	41–53
PBT	+	+	+	220–250	39–60
PBS	+	+/-	+	120–140	19–34
PC	++	+/-	++	275–285	57–72
PMMA	+	-	+	280–250	52–70
HDPE	+	+/-	+	120–150	11–45
PP	+	+/-	+	130–170	9–80
PVC	+/-	+/-	++	200–300	1–59
TPU	+/-	+	+	210–225	6–33
PEI	++	+	++	350–390	69–81
PEEK	++	+	++	360–450	48–265
PPSF	++	+	+/-	350	55
PEKK	++	+	++	350	90–110

done to overcome the problems of increased porosity and stress concentration [3].

Numerous mathematical and statistical studies have been carried out to produce specimens correctly and get high-quality results. Some parameters that influence the quality of printed components are described here and are represented in Fig. 7.

## 2 Filament-Based Material Extrusion

In the initial periods of additive manufacturing, STRATASYS created and copyrighted Material Extrusion, often referred to as FDM or FFF. In 2009 when the patent expired, this technique was essential in the growth of the consumer 3D printing sector and the industry's widespread acceptance of additive manufacturing. As discussed in the Introduction section, a filament-based 3D printer utilizes a continuous supply of filament made from thermoplastic polymer. A movable heated printer extruder head, sometimes referred to as an extruder, feeds the filament from a coil. The head of the extruder is computer controlled; the material is layered on top of the current layer, following a tool path specified by the component cross-sectional boundaries. Once a layer is completed, the bed descends a layer thickness height, and the nozzle continuously supplies semi-molten material to fill the specified boundaries until wholly filled, resulting in a complete three-dimensional structure.

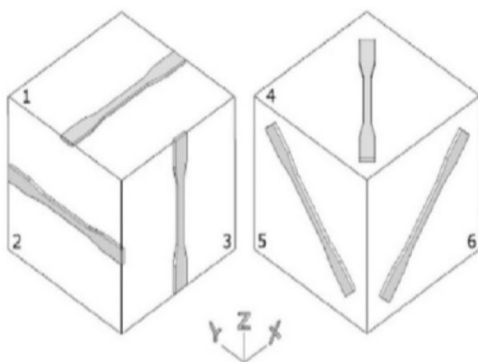
There is an ongoing necessity to enhance product quality in all production processes. Many factors influence the product's aesthetics and mechanical qualities. As a result, optimizing important parameters to reduce errors throughout the printing process is critical in obtaining excellent quality.

- The filling pattern substantially influences the mechanical characteristics and stiffness of printed components. It is available in a variety of shapes and geometries. The shape of components could be hollow or solid, determined by the infill percentage. The infill percentage varies between 0 and 100% [46]. Linear, cubic, honeycomb, rectilinear, or wiggly patterns are possible [47].
- The temperature of the nozzle is another critical parameter, which varies from 170 to 220 °C depending on the polymer's melting point. The inappropriate nozzle temperature affects the process of printing and layer bonding.
- The temperature of the printing bed is another important factor in controlling the 3D-printed product quality. Based on the material characteristics, the range of temperature varies from 0 to 80 °C.
- The diameter of the nozzle impacts the product's surface quality and mechanical capabilities. The nozzle diameter ranges in size from 0.2 to 0.8 mm. Printing with a narrower nozzle diameter produces more exact results, but it takes a longer printing time [48, 49].
- The importance of build orientation in material extrusion additive manufacturing cannot be understated. This parameter impacts mechanical characteristics and surface

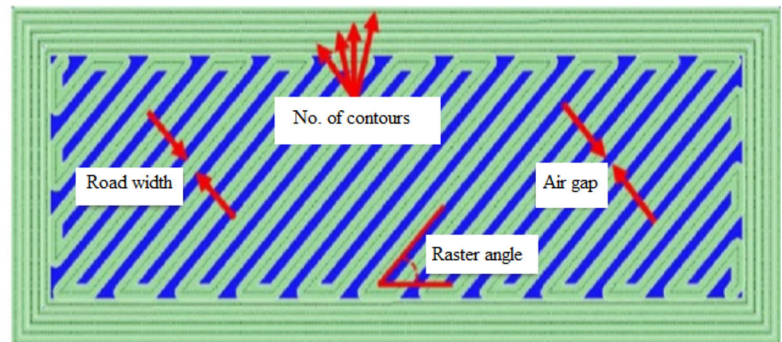


Fill pattern	first mode	second mode	third mode	Fill pattern	first mode	second mode	third mode
Line				Concentric			
Rectilinear				Honeycomb			
Grid				3D honeycomb			
Triangle				Hilbert curve			
Star				Archimedean chords			
Cubic				Octagram spiral			

(a)



(b)



(c)

Fig. 7 a Filling pattern; b build orientation; c Raster angle and raster width [51]

texturing [10]. Objects can be deposited from any angle ( $0^{\circ}$ – $180^{\circ}$ ) and in any direction ( $x$ ,  $y$ , and  $z$ ).

- The air gap is the distance between neighboring rasters, FDM beads, and the same layer. For the 3D-printed components, tensile strength is affected by the air gap and the orientation. For the components fabricated by 3D printing, stiffness and strength were improved by an air gap of ( $-0.003$ ) [50].
- The material bead width and the angle of the  $x$ -direction raster pattern are referred to as raster width and raster angles, and these variables cause warping and shrinkage.

Experiments revealed that as road width, layer thickness, contours, and air gap decrease, the percentage change in part width reduces accordingly [50].

- Layer thickness is the separation between the nozzle and the platform, which determines the height of every layer. This factor significantly impacts the surface roughness of components and the time required for printing [52]. The thickness of the layer ranges from 0.06 to 0.6 mm. Product quality is improved, whereas the time of printing is extended by reducing the layer thickness.

## 2.1 Studies Related to the Single Material Printing System

Mireles et al. modified the liquefier design from curved to straight for eutectic Bi58Sn42 and non-eutectic Sn60Bi40 controlled deposition to observe the effects of the modified deposition [53]. In the modified design, as shown in Fig. 8, the 90° bend is removed for the transient response of the stepper motor, reduced driving force by reduced pressure, and improved heat transfer to achieve a slight temperature gradient between the liquefier inlet and outlet. The pressure was significant because it directly impacts how well the material is controlled during deposition, the magnitude of force required to extrude the material filament increases with the increase in pressure drop. The modified design observed that the pressure drop is 14% lower, and hence the feed force for continuous deposition was reduced by 150%. Further, experiments show the temperature difference for the original liquefier was 65 °C and for the modified liquefier was 48 °C demonstrating that accuracy has improved. Simulation results of both designs emphasize the need for a straight extrusion head, and it also minimizes friction, slips between the filament and liquefier walls, and unequal heat distribution, which all constitute non-ideal conditions. Microstructural analysis of FDM-built Bi<sub>58</sub>Sn<sub>42</sub> shows lamella coarsening because of preheating current layer by the previously deposited layer. This coarsening effect improves the mechanical properties Sn-Bi alloy. Electric circuits improve conductivity as coarse grains offer less resistance to the flow of electrons than refined grains. The results of this work can serve as a reference for the development of an FDM printer for high-strength alloy. Nowadays, most FDM printer employs a straight liquefier.

One of many gaps in additive manufacturing is the inability to provide real-time relevant data due to the lack of sensors. In the work carried out by Coogan and Kazmer, a customized pressure transducer and a thermocouple for assessing the temperature of the produced melt are designed and described by modifying the nozzle for in-line rheological measurements for the first time [54]. There are incorporation of sensors for in-line rheometer design and development, presentation of temperature, pressure, and viscosity within printing nozzle, and then validation against traditional rheometer for polycarbonate (PC) and high-impact polystyrene (HIPS). Some incorporated rheological corrections are non-Newtonian corrections, entrance effects, temperature fluctuations/inaccuracies, pressure effects, and shear heating. For measuring melt-pressure, a pressure hole (Fig. 9a) is provided in the nozzle, load transfer column (Fig. 9b) with a thermocouple is inserted in the pressure hole (Fig. 9c, d) for measuring melt temperature and transfer of load from melt to customized clamp (Fig. 9e). The melt load is transferred to a 10-lb load cell by the customized clamp

(Fig. 9f). The voltage then converts the melt pressure from the load cell.

The data acquisition device (DAQ) counts pulses from the stepper motor, which drive the filament feeding gear, and the encoder, which makes contact with the filament; four thermocouple measures temperature. A stepper motor was used for the filament, having 830 pulses/mm, and pulses were sent to DAQ by a microcontroller every time the motor was set in operation to measure the extrusion rate. It may not be accurate because of some slipping; hence an encoder was used.

Data gathered from the sensor must be translated into an apparent shear rate and shear stress at the wall to determine the apparent viscosity. For that volumetric flow ( $Q$ ) rate is calculated by Eq. (1)

$$Q = \dot{V} \times A = \frac{v}{\zeta} \times \pi R_{\text{fil}}^2 \quad (1)$$

where  $\dot{V}$  is the filament velocity,  $A$  is filament area,  $v$  is pulse per second,  $R_{\text{fil}}$  is filament radius and  $\zeta$  is pulses/mm. The following equation was used to obtain the adjusted apparent shear rate [55, 56].

$$\Gamma = \frac{4Q}{\pi R_{\text{noz}}^3} \quad (2)$$

Equation 3 gives wall shear stress

$$\tau_w = \Delta p \times \frac{R_{\text{noz}}}{2L_{\text{noz}}} \quad (3)$$

In Eq. (2),  $R_{\text{noz}}$  and  $L_{\text{noz}}$  are radius and nozzle tip length, respectively.

Rheological modeling was done by adopting the temperature-dependent Cross–Williams–Landel–Ferry model [55] for estimating viscosity at zero shears. The Bagley adjustment was made by measuring the viscosity to compensate for end effects (these include entry effects upstream to the nozzle tip from the conical cylindrical taper and exit effects) [56]. To compensate for the non-Newtonian nature of the polymer, Rabinowitsch correction was used [13]. The Barus equation can compensate for the viscosity dependence on pressure [57].

The developed FDM rheometer can measure viscosity very accurately, as confirmed by comparison with the already established rheometer as shown in Fig. 10, and it can measure viscosity for a wide range of temperature and shear rates. The above-mentioned adjustments for viscosity measurements are consistent with already-developed rheometers. The influence of all adjustments is the decreasing order as Bagley end effects → Rabinowitsch → Temperature inaccuracies → Pressure effects.

**Fig. 8** **a** Original liquefier; **b** modified liquefier [53]

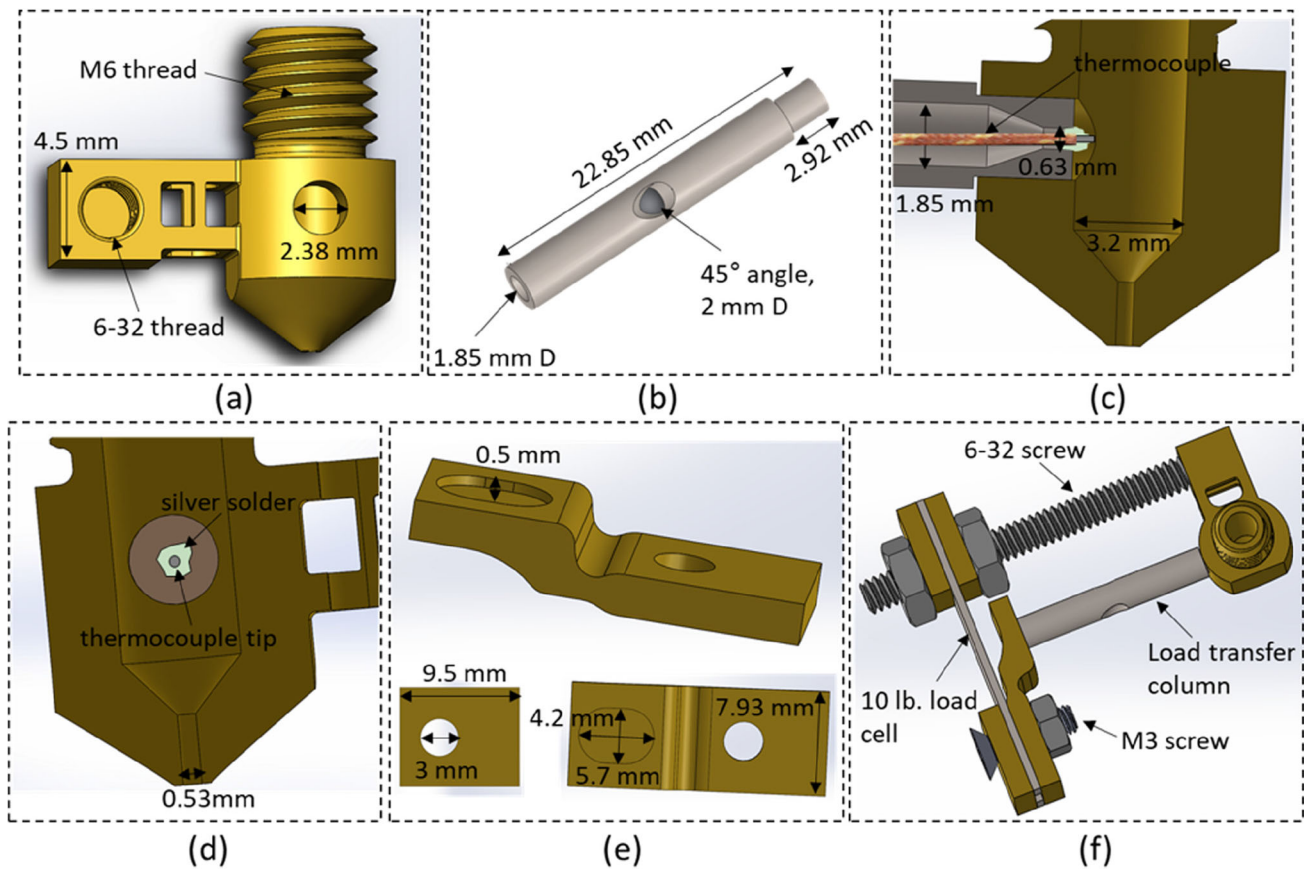
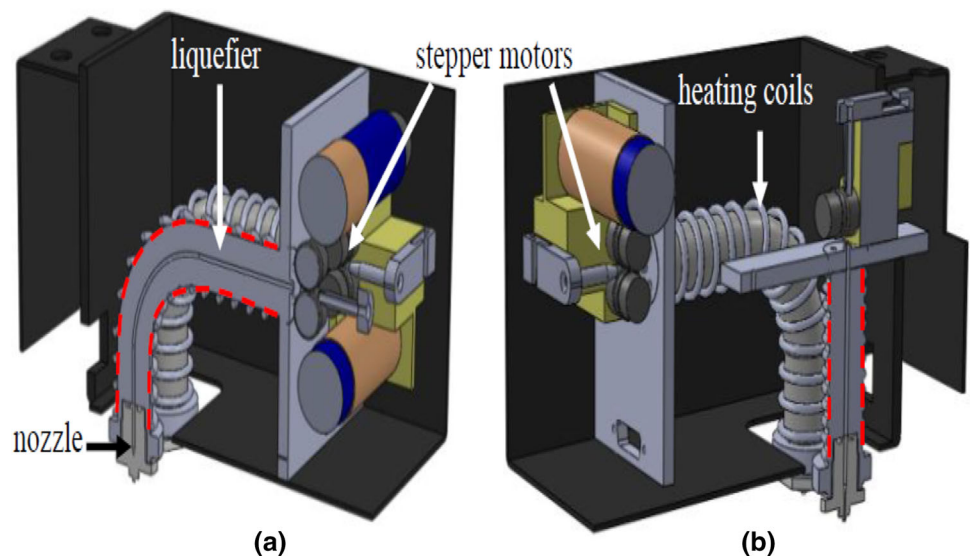
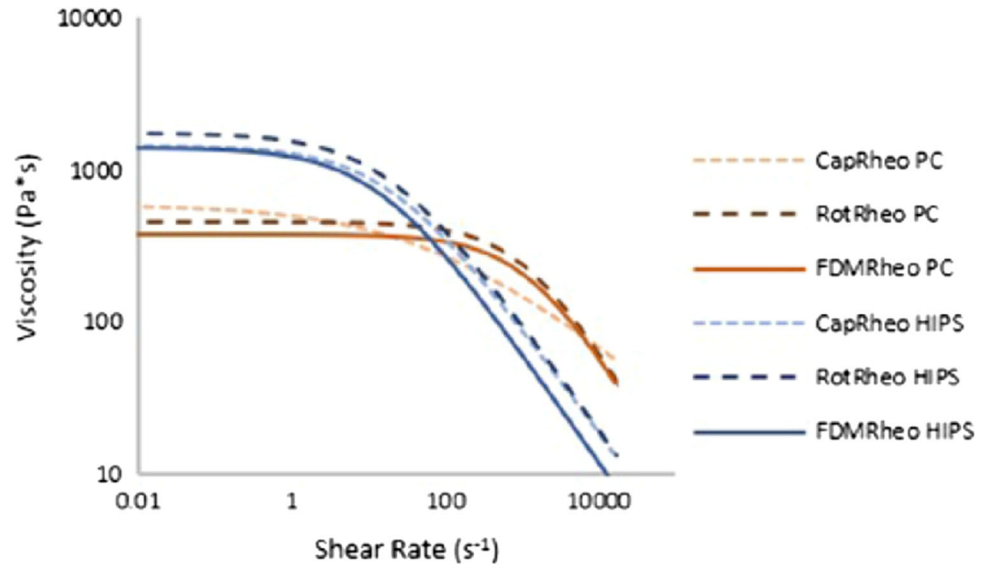


**Fig. 9** Design of nozzle: **a** customized nozzle, **b** transfer column for load, **c** and **d** load transfer column, inside the pressure port of nozzle a thermocouple is inserted, **e** customized clamps, and **f** complete assembly [54]



**Fig. 10** Comparison of Cross-WLF models for PC and HIPS at a temperature of 260 °C by the three rheometers [54]



Park et al. [24] developed a material extrusion-based additive manufacturing system with the capability to maintain the high temperature of the extruder and chamber for printing the defects-free parts of super engineering plastics, namely polyether ether ketone (PEEK). They demonstrated the feasibility of utilization of high-performance engineering plastic 3D-printed parts in the industries; by optimizing thermal process parameters for mechanical strength. The filament is fed through the heating zone, which is encircled by a heating block, in a conventional extruder design before being extruded out of the nozzle. In this design, a substantial amount of heat flows upward and makes the filament flexible and flabby which results in discontinuity in material extrusion. In addition to the finned heatsink, Park et al. [24] employed a blower fan and an airflow duct to lessen the upward heat flow. They also altered the heating zone to print high-temperature polymers like PEEK and polycarbonate (PC). The length of the heating zone was reduced to 10 mm for successfully printing the part at 400 °C. According to their research, the created extruder produced the object with a better tensile strength than the extruder's standard version because it had a shorter and more concentrated melting zone.

Xiaoyong et al. [23] investigated the impact of several process variables on the mechanical characteristics and printing accuracy of PEEK-printed objects, including bed temperature, ambient temperature, and infill density. Their observations show that optimized process parameters improve the mechanical properties of the parts. They achieved the maximum tensile strength of PEEK at 77 MPa, higher than the tensile strength of PLA.

The impact of build orientation on the mechanical and thermal characteristics of FFF 3D-printed items was examined by Zaldivar et al. [32]. They used identical FFF

3D-printed dog bones with six different orientation angles and observed the variation of tensile strength, coefficient of thermal expansion, failure strength, poisons' ratio, and modulus. They characterized 3D-printed items with their injection molded equivalents in terms of their mechanical and thermal characteristics. When compared to injection molded components, it is discovered that the tensile strength and failure stresses of FFF 3D-printed parts range from 46 to 85% and 2 to 7%, respectively. They concluded that the part printed in a particular build orientation which has more fibers aligned in the load direction shows higher strength.

To produce high-quality components, it is necessary to detect filament breaking. The mechanical contact switch filament breaking detection technique has a limitation in that when the filament is broken, it is still in contact with the hole, and its detection is difficult. In this work, the Acoustic Emission (AE) technique is used, which has the advantage that it can detect even bursting and weak signals even from complex backgrounds [58].

Feed rate, which is a crucial factor in building quality, can be approximated by Eq. (4) [59, 60].

$$v = \frac{Q}{WH} \quad (4)$$

Feed rate is  $v$ ,  $Q$  is volumetric flow rate,  $W$  is bead width, and  $H$  is slice thickness.

$Q$  can be approximated as a function of nozzle geometrical parameters, nozzle pressure  $P$ , material viscosity  $\eta$ , nozzle diameter  $D$ , and nozzle's conical length  $L$  as in equation no. (5) [61]

$$Q = \frac{\pi \left(\frac{D}{2}\right)^4 P}{8\eta l} \quad (5)$$

Pressure  $P$  placed on the filament affects the critical feed rate given by Euler buckling analysis in Eq. (6) [62].

$$P = \frac{\pi^2 E d^2}{16 L^2} \quad (6)$$

For the filament,  $E$ ,  $d$ , and  $L$  are Young's modulus, diameter, and length from pinch rollers to liquefier entry. The critical feed rate can be obtained from Eqs. 4, 5 and 6.

A lower feed-to-flow ratio implies that material is being extruded more rapidly than the filament is moving. This causes an increase in layer thickness and a slow accumulation of extrudate across the nozzle, which usually results in clogs. Unless this problem is not rectified, a filament break follows, with a part of the filament stuck within the extruder [63]. This work proposed acoustic emission representation on the probability distribution shape. The conducted work consists of the relative similarity and skewness of the AE signal.

**Instantaneous skewness**—The third standardized moment is determined to quantify the asymmetry of a real-valued random variable's probability distribution regarding its mean.

Relative similarity  $R_S$  represents the difference between the probability distribution of two acoustic emissions.

The electric motor, printing head, extruder head, and friction between the pinch roller and filament are the significant sources of acoustic emission signals during printing. The extruder generates a weak signal; hence, sensor should be placed close to it. An emission transducer and an acoustic emission acquisition system were used for acoustic preamplifiers to measure acoustic emission signals. The transducer's operational range was 100–1000 kHz, and the operational temperature range was 65–175 °C. The frequency of sampling recording waveforms was 5 MHz. The preamplifier was used for the 40-dB gain of waveforms.

Spectrum analysis was performed by conducting a test on two machines. Test #1 on Stratasys uPrint, test #2 on JG Aurora model. Graphs were obtained for both steady fabrication and breakage conditions. Instantaneous skewness is calculated by Eq. 7, where  $x(n)$  is the  $n$ th section's amplitude value.

$$\gamma_{\text{instant}}(n) = \frac{E[x^3(n)] - 3E[x(n)]E[x^2(n)] + 2E^3[x(n)]}{(E[x^2(n)] - E^2[x(n)])^{\frac{3}{2}}} \quad (7)$$

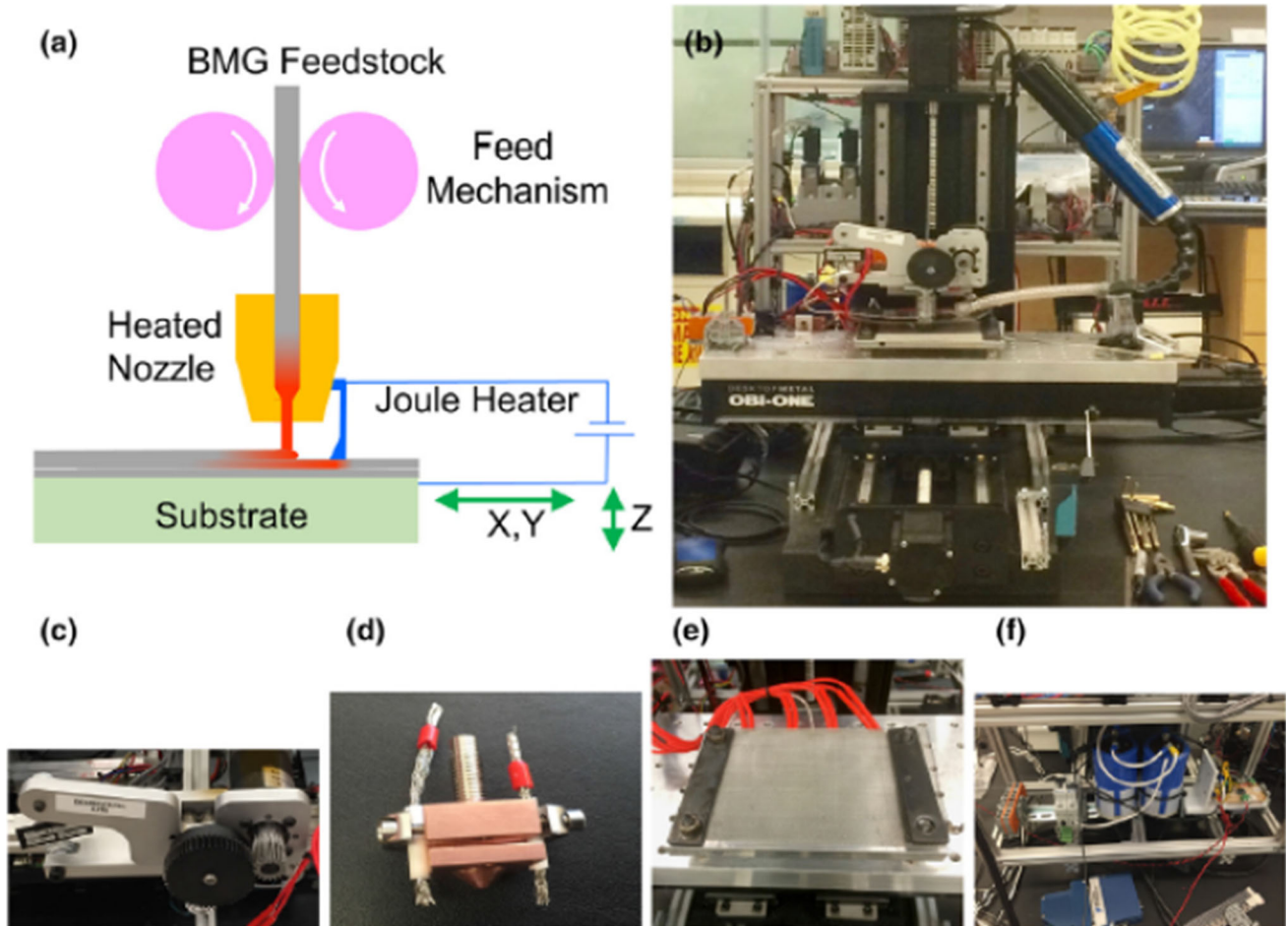
During steady-state friction was weak; hence, acoustic emission and after filament breakage friction increases because of constant rubbing with the pinch roller. Relative similarity values for steady-state activity are closer to one as acoustic signal closely resembles reference signals, decreasing after breakage. The coefficient of variation of skewness values is higher than relative similarity, which suggests that

skewness is more sensitive to filament breakage. This work provides an appropriate way for on-site process parameters surveillance of FDM.

AM of metals requires metals in powder-form and then concentrated heating and solidification are done by electron or laser beam. These methods are costly as they require intensive energy sources, atmosphere control, grain control of powder, and post-processing for dimensional accuracy. This work is carried out to overcome the limitation of 3D printing for metals as they lack continuous softening with temperature, unlike thermoplastic [64], demonstrating extrusion-based 3D printing of bulk metallic glasses (BMGs). BMGs have an amorphous structure, high strength, high toughness [65, 66], and high corrosion resistance [67]. Above glass transition, BMGs relax into liquid-like thermoplastic and can be used in the FFF process, as shown in Fig. 11.

Zr<sub>44</sub>Ti<sub>11</sub>Cu<sub>10</sub>Ni<sub>10</sub>Be<sub>25</sub> was selected as the production material because of its widespread availability and thermoplastic formability. BMG rods with a diameter of 1 mm up to a length of 70 cm were used. When the material was extruded at 460 °C, the crystallization time was 100 s, and the viscosity was 10<sup>5</sup> Pa.s. When the temperature is low, the extrusion force is high, and the processing time is short at high temperatures. Nozzle diameter is 0.5 mm and printing speed 5 cm/s. Printing was carried out with a crystallization time of 1 day [68] on stainless steel mesh preheated to 400° C. All aspects of printing are carried out in the air. A wide variety of BMG parts were printed using the approach outlined in Fig. 12. The volumetric flow rate of 10 mm<sup>3</sup>/s was obtained as compared to 1–10 mm<sup>3</sup>/s for laser powder bed fusion [69, 70] and 40 mm<sup>3</sup>/s for thermal spray [71]. The needed feed force while printing is below 100 N; however, it needed to rise to 1000 N during start-stop operations. Thermal analysis indicates that the difference in temperature  $\Delta T$  between the temperature of the glass transition  $T_g$  and the temperature of crystallization  $T_x$ , crystallization heat  $\Delta H$ , for supplied BMG is  $T_g = 371$  °C,  $T_x = 473$  °C,  $\Delta T = 102$  °C,  $\Delta H = 83 \pm 5$  J/g, and for extruded BMG that is  $T_g = 373$  °C,  $T_x = 476$  °C,  $\Delta T = 103$  °C,  $\Delta H = 85 \pm 5$  J/g. Mechanical analysis shows that when printed BMG is tested with loading parallel to BMG, printed layers fracture strength is 1220 MPa compared to 790 MPa when tested with loading perpendicular to BMG printed layers. Results obtained are very similar to commercially available technologies and there is scope for development of potential fused filament fabrication of BMG's.

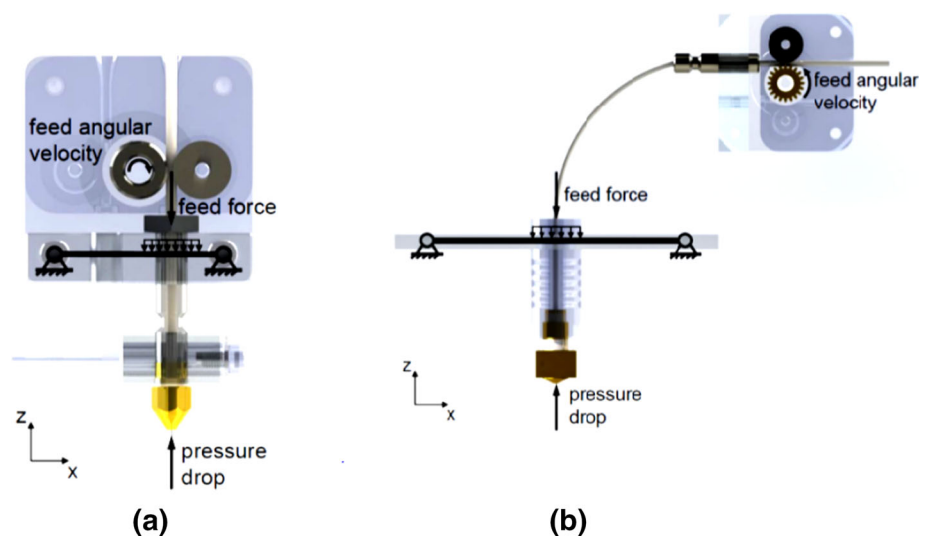
Nozzle clogging is among the most common FDM process errors. The printed parts' consistency is adversely affected by surface roughness, geometric tolerance, or mechanical properties. Nozzle monitoring is developed using vibration sensors [72]. Firstly, bar mount that supports the liquefier is modeled as a beam (Fig. 12), and then a simulation for



**Fig. 11** Process summary. **a** Schematics of extrusion of BMGs by FFF. **b** BMG printer set up. **c** Feed mechanism employed to generate 1000 N force. 5 cm/s is the maximum extrusion speed. **d** Joule heater attached to an Extrusion nozzle. The Joule heater was powered by an energy supply

(48 V, 72 A). **e** The substrate stage was heated to 400 °C to facilitate initial bonding on the substrate of fabricated BMG. **f** Capacitor bank of 1F [64]

**Fig. 12** Beam-modeled layout for **a** direct; **b** Bowden FFF extruder [72]





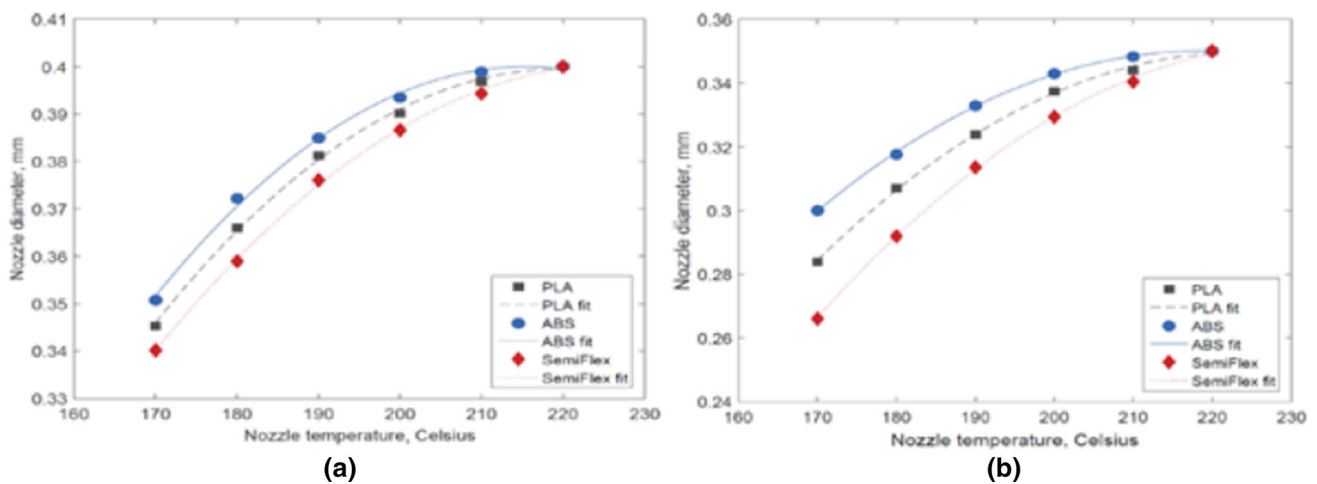


**Fig. 13** Nozzle diameter during partial clogging for direct and Bowden extruder [72]

nozzle clogging was carried out. This was done for partial solidification by reducing the temperature of the nozzle.

There are mainly two types of force in FFF: back pressure and feed force. Feed force depends upon unsupported filament length, filament feed, filament properties, motor torque, and drive gear parameters, while back pressure force depends upon pressure drop in a heated liquefier. Force due to back pressure is the summation of all pressure drop force over nozzle length.

Assuming uniform properties of the material and a constant cross section for the Euler–Bernoulli beam, the bar mount system can be modeled as a simply supported beam having a partly uniformly distributed load or both ends pinned. Using a vibration sensor to monitor nozzle performance necessitates mounting the accelerometer onto the extruder’s bar mount. Since the extruding system is generally moving in printers, it adds additional complexity to vibration measurement. To overcome this problem, immovable extruder and movable printing bed were used. Firstly, to keep track of nozzle performance monitoring, both Bowden and direct type of extruding systems were used separately to measure vibrations. Secondly, strands of materials including ABS, PLA, and SemiFlex of 1.75 mm diameter and tolerance of  $\pm 0.05$  mm were employed. Finally, strands of three materials were extruded separately using Bowden and direct extruder system, whereas the temperature of the extrusion was adjusted from 220 to 170 °C having a 10 °C step size. Significantly, reducing the temperature of the nozzle during extrusion was only utilized to simulate nozzle clogging since lowering the nozzle temperature of the nozzle solidifies the strand around the internal surfaces of the nozzle, resulting in a drop in filament diameter. Nozzle diameter during partial clogging is graphically represented in Fig. 13. A comparison between theoretical and experimental data establishes the usefulness of a nozzle monitoring system.

## 2.2 Studies Related to Multiple Material Printing Systems

The most traditional 3D printer uses only a single color filament, limiting the use of 3D printing, one way to overcome this is to carry out different color mixing. It is difficult to simultaneously 3D print several materials, such as polymers, metals, and semiconductors at greater resolutions. In addition, existing high-speed 3D fabricating techniques face challenges due to the accurate arrangement of discrete and continuous regions required to ensure both electrical connectivity and device performance. The work of Loke et al. described the use of filaments made of various materials ordered in intricate microstructures along with an exterior adhesion promoter to 3D fabricate high-quality interactions and a variety of topological results [73]. The capability of the FDM technology to expand the design beyond complicated geometries is demonstrated by recent developments in multi-material 3D and 4D printing (time being the fourth dimension). Due to the roots of 4D multi-material fabrication in 3D, it faces some of the same difficulties as 3D fabrication, including a restricted materials selection, poor printing resolution, mechanical characteristics, and limited dimensional stability [74].

In the work of Han et al., the 3D design of the nozzle is carried out by UG software [75]. Studies are carried out by simulation for the optimum feed speed of filament at various temperatures, which are later verified by experiments. The conjunction of the temperature field and feed speed of filament on the distribution of the pressure field and the velocity field is the basis of a brief analysis of the hole and intersection of the nozzle. Nozzle assembly consists of a heating block, fixed block, throat pipes, and nozzles, as shown in Fig. 14. The throat pipe, nozzle thread hole, thermistor hole, and pipe hole for the heater are components of the heating system.

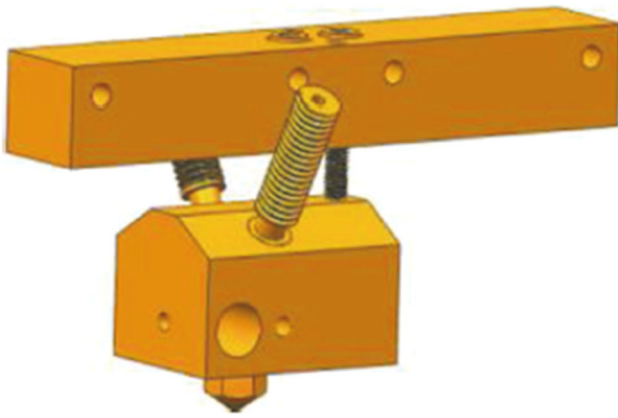


**Fig. 14** Assembly of the entire model [75]

Using screw threads, the nozzle, thermistor, and throat pipe are connected to a heating system. In the hole of the heating pipe, a heater is attached directly, and the heating pipe is attached to a threaded hole with screws. The heating block throat is assembled in the pipe thread hole, and the nozzle is inserted and tightened into the hole of the nozzle thread.

Boundary conditions are set for both the inlets; ABS filament of 1.75 mm diameter with an initial temperature of 25 °C, and outlet is set to flow boundary. The color mixing effect depends upon whether, at the intersection, both the filaments can be melted entirely or not. Simulation and analysis of the temperature field of two filaments are carried out by changing the feed speeds of the filaments.

At 0.2 mm/s velocity: the feed speed of both the filaments is 0.2 mm/s, the initial temperature is 298.15 K, the boundary temperature is 493.15 K simulation time is the 60 s. After the 50 s, the temperature inside the flow channel is considered steady when ABS entry is 10 mm, lowest temperature of 484.8 K is reached at the filament center, which is below the test temperature for easy extrusion. Temperature is raised to 503.15 K for melting of filaments at the intersection now; the temperature at the intersection is 494 K which is sufficient for smooth extrusion. At 0.5 mm/s velocity: the feed speed of both the filaments was 0.5 mm/s, the initial temperature of 298.15 K, the boundary temperature of 503.15 K, and the minimum temperature at the intersection was 489 K, and extrusion can occur smoothly. At 1 mm/s velocity: for both the filaments, the feed speed was 1 mm/s, initial temperature 298.15 K, and boundary temperature 508.15 K. The lowest temperature of 485 K was obtained, which is below the test temperature. For easy extrusion, the wall temperature was raised to 513.15 K; now lowest temperature obtained was 489 K, but the filament temperature by adding heat became higher faster, which resulted in premature softening of filament; hence filament feed speed of 1 mm/s was not recommended. To check the feasibility of the device at 220 °C and 230 °C, selected filaments were printed as a cylinder of

10 mm diameter and 10 mm height. At 220 °C, the filament was not melted completely, and under continuous feeding, the filament slid and resulted in blockage at the intersection. At 230 °C, the molten filament accumulation phenomenon was observed. Through test verification, faults in design are found, and to eliminate blockage and risk; the design needs to be improved in the future.

Conventional FFF has a limitation of printing only one type of color at once, resulting in a time break in switching the filament of different colors; to overcome this multi-nozzle extrusion system is designed. The model designed by Abilgazyev et al. [76] has five nozzles that can print five colors without any manual interruptions for changing the filament. Print time, frequent maintenance, and cleaning can be reduced using this setup. Figure 15a shows that the developed extruder has mainly a two-section hot end and cold end, filament driven. Five nozzles are present in the hot end for five different colors; the cold end has five holes cylinder for five colors of filaments, thrust bearings, stepper motor, and gears. As depicted in Fig. 15a, b mechanism is employed for suitable contact with hobbled shaft and filament, and the filament is pushed toward the shaft by the mechanism so that friction increases. A Bowden cable connects the cold end to the hot end, ensures a steady filament supply, and helps in weight reduction. ABS was selected as the material of plates for its light weight and high strength properties of ABS. Finite element analysis was carried out to check its applicability, and simulation results showed a factor of safety of 8.1, which is well above the widely accepted factor of safety of 1.5.

In the continued work from previous literature, this work was carried out by Ali et al. to overcome FFF's typical limitations of printing with different colors, reducing the time of printing, efficient use of motors, and reducing the time of printing weight and manufacturing cost [77]. The conceptual design of this model is the same as depicted in Fig. 15, which has the following parts;

- Cold end design: cold end has a five-hole cylinder for five colors of filaments, thrust bearings, stepper motor, and gears.
- Plate design: two plates were used, and all other components were fixed. It performs two main functions hold all elements and carry their weight. Earlier, gypsum was used, but PLA was selected as the material for plates because of bending.
- Pushing mechanism: a pushing mechanism is employed for suitable contact with hobbled shaft and filament, which pushes the filament toward the shaft to increase friction. An earlier spring system was used, but it resulted in filament degradation and was replaced with a lever mechanism.

Minimum torque is required to rotate the cylindrical probe, which is calculated, as the minimum mass required was 90 g,

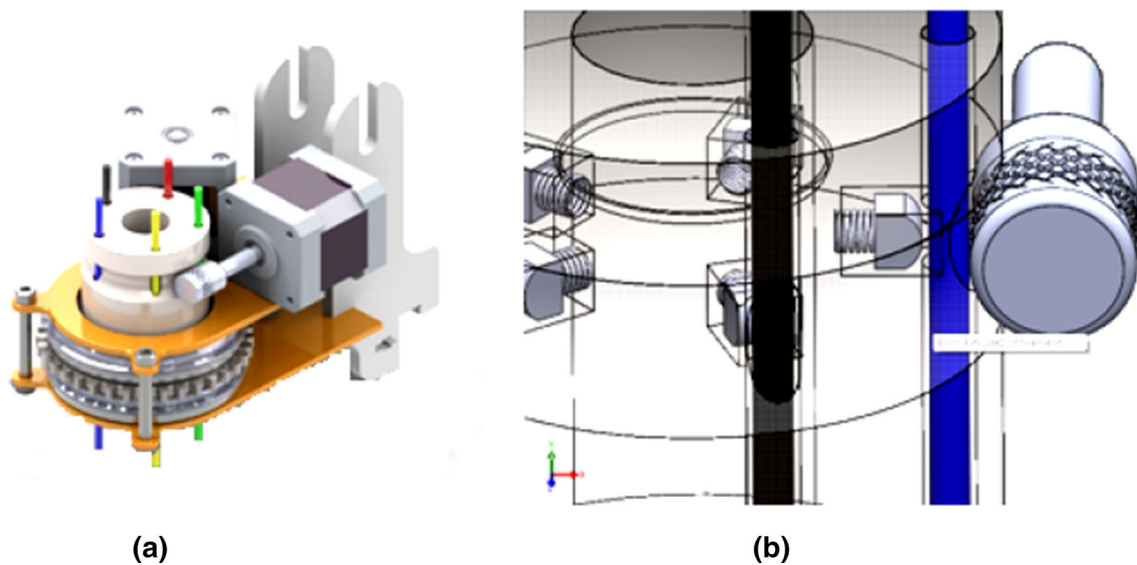


Fig. 15 a Cold end design of extruder; b pushing mechanism [76]

equivalent to 0.8829 N. Torque  $T = F * R$ , where  $F$  is force and  $R$  is pitch circle radius of larger gear,  $T$  is 44.145 N mm. Spur gears were used as they are easy to manufacture, and also, speed is low for them to use. The pitch circle of the larger gear used is 100 mm, equal to the thrust bearing diameter. A smaller gear may reduce friction and increase wear between parts if used. The module was 1.25 mm; teeth on larger and smaller gears are 80 and 20, respectively. Gears were designed for bending using the Lewis equation given by Eq. 8.

$$\sigma = \frac{F_t}{K_v b Y m} \tag{8}$$

where  $F_t$  tangential tooth force (N),  $K_v$  the velocity correction factor,  $b$  is tooth width (mm),  $m$  is gear module (mm),  $Y$  is Lewis form factor, and  $\sigma$  bending stress in gear (MPa). Using Eq. 17, the widths of the pinion and gears were calculated as 8 mm and 10 mm, respectively. A prototype was tested for the following parameters;

- Changing the guided filament by rotational motion: rotational motion was steady and hence verified the usefulness of the gear pair and bearing.
- Driving the chosen filament: the filament does not come into contact with strong frictional forces, which could cause it to cease moving.
- Placement and movement of the hot end: five hot-end heads with insulating fins were installed correctly on the top of the holding construction. The hot-end arrangement was solid and lightweight.
- Extrusion of filament: the pulse per minute must be set to regulate the filament flow, and the counter-delays must be

factored into the calculations. The maximum speed of the filament can be set depending on the travel required per minute.

- Structural rigidity: for the cold-end arrangement, several flaws were observed for structural rigidity. Bending stress deflection because of the two stepper motors' combined weight was observed in the upper plate made of PLA.

The proposed model gives a suitable method of 3D printing for five colors using only two stepper motors. Comparison with existing multi-nozzle extruders and results obtained are represented in Table 3.

The work of Lopes et al. addressed the boundary interface or the contact produced at the geometric border of various materials, which is among the most significant problems in multi-material 3D printing [78]. Three different types of tensile test samples were fabricated: (A) a sample made of one material and fabricated using only one extruding head; (B) a sample of one material having multi-sections fabricated using two extruding heads arranged in a zebra pattern, and (C) a multi-material sample fabricated in a zebra-crossing arrangement using two different materials. A reduction in tensile strength and Young's modulus was observed in all of the zebra crossing samples. This decrease in performance, particularly in terms of tensile strength, was primarily caused by boundary interfaces created by the switching of the engaged extruding head. These interfaces caused an intense inconsistency in the test samples than was fostered by the process-inherent interactions between nearby fabricated filaments. The study of Waly et al. [79] examined how varied interlayer lengths and thicknesses affect crack development in multi-material 3D-fabricated polymers at various loading levels. Their research findings are: (A) as far as the

**Table 3** Performance comparisons [77]

Model	No. of filament colors	No. of motors	Weight on moving rails (kg)	Cost	Operational pauses
Single-nozzle “Prusa i3”	1	1	0.49	500	Long
The Kraken model	4	Not known	Not known	Not known	Short
Theta 3D printer	4	10	0.4	Not known	Not known
RoVa3D printer	5	5	0.2–0.05	> 3500	Short
Multi-extruder NPr2	<6	2	0.15–0.25	Not known	Medium
Proposed prototype	5	2	0.18	700–1000	Short

build orientations, loading levels, and mechanism of fracture are the same, the interlayer thickness has little impact on the fracture toughness; (B) with the increase in loading levels fracture toughness of composite was found to increase.

In the study of Ahmed et al. (process parameters), ABS and carbon fiber-reinforced polylactic acid were combined to form laminar composite structures [80]. Their research examines the impact of different printing parameters on the developed composite’s interfacial bond strength (IFBS) using the surface response approach. Two failure mechanisms were identified during the physical assessment of the examined specimens, one mode of failure having a significant IFBS due to material patch migration and another mode of failure having low IFBS with no patch migration. ANOVA showed that the pattern of the printing process parameters was quite interactive. After rigorous testing, their study concluded that the middle range of printing speed, greater filling density, and low layer thickness are responsible for the effective IFBS.

In the work of Quero et al. [81], a microchip capillary electrophoresis (MCE) was made for the first time using the FDM. Three conducting polymer filaments including copper, carbon black, and graphene were used to embed electrodes for capacitively coupled contactless conductivity detection ( $C^4D$ ) into the MCE. Two-extruding-nozzle FDM printer was fabricated for one-step multi-material 3D fabrication with optimized parameters embedding MCE- $C^4D$ . The traditional MCE design was selected, and PETG material was used to fabricate the main section of the MCE- $C^4D$  device. Four reservoirs of solution (background electrolyte, sample, and auxiliary), a separating microchannel, and injecting microchannels were included in this microfluidic design (Fig. 16a). The system comprised four 3D-printed layers both above and below the microchannels, exclusive of solution reservoirs (Fig. 16b). Two built-in electrodes were also included in the 3D-fabricated MCE system placed 0.8 cm apart in the separating channel to carry  $C^4D$  (Fig. 16c). As

shown in Fig. 16d, the electrodes were successfully 3D fabricated by the main section of the device using conducting filaments. Figure 16e depicts the final 3D fabricated MCE- $C^4D$  device.

### 3 Pellet-Based Material Extrusion

The most popular method is freeform filament extrusion printing, but there are a limited number of available materials in the filament form. Some materials cannot be converted into filaments, such as biopolymers, materials having high carbon fiber. For the first time, Bellini explored pellet-based extrusion additive manufacturing, also known as screw-assisted extrusion additive manufacturing, in 2002. Initially, developed systems were used mainly in the field of biomedical AM. In 2014, pellet-based extrusion additive manufacturing systems were developed for many applications. By the year 2016, small-scale printing of this system was successfully employed by systems including 3D Discovery<sup>®</sup> [82], PAM<sup>®</sup> [83], M3DIMAKER<sup>®</sup> [84], and ExAM 255<sup>®</sup> [85]. Large-volume printing started in 2016 when robotic arm-based systems were developed because of the higher degree of freedom and capability. Large-volume printing systems are BAAM<sup>®</sup>, Gigabot X<sup>®</sup> [86], and Discovery<sup>®</sup> [87].

The quality of components produced by this technology depends mainly upon process parameters adopted for printing. The most critical process parameters in pellet-based material extrusion are screw speed and barrel temperature. Barrel temperature is the surface temperature of the barrel. The screw speed determines how long the material is exposed to heating systems. Kumar et al. studied the impact of screw rotational speed and barrel temperature on melt flow speed and cross section of deposited filaments [88]. It was observed that as screw rotation speed and barrel temperature were increased, melt flow speed increased. This occurred because the pressure gradient increased as the screw speed increased,



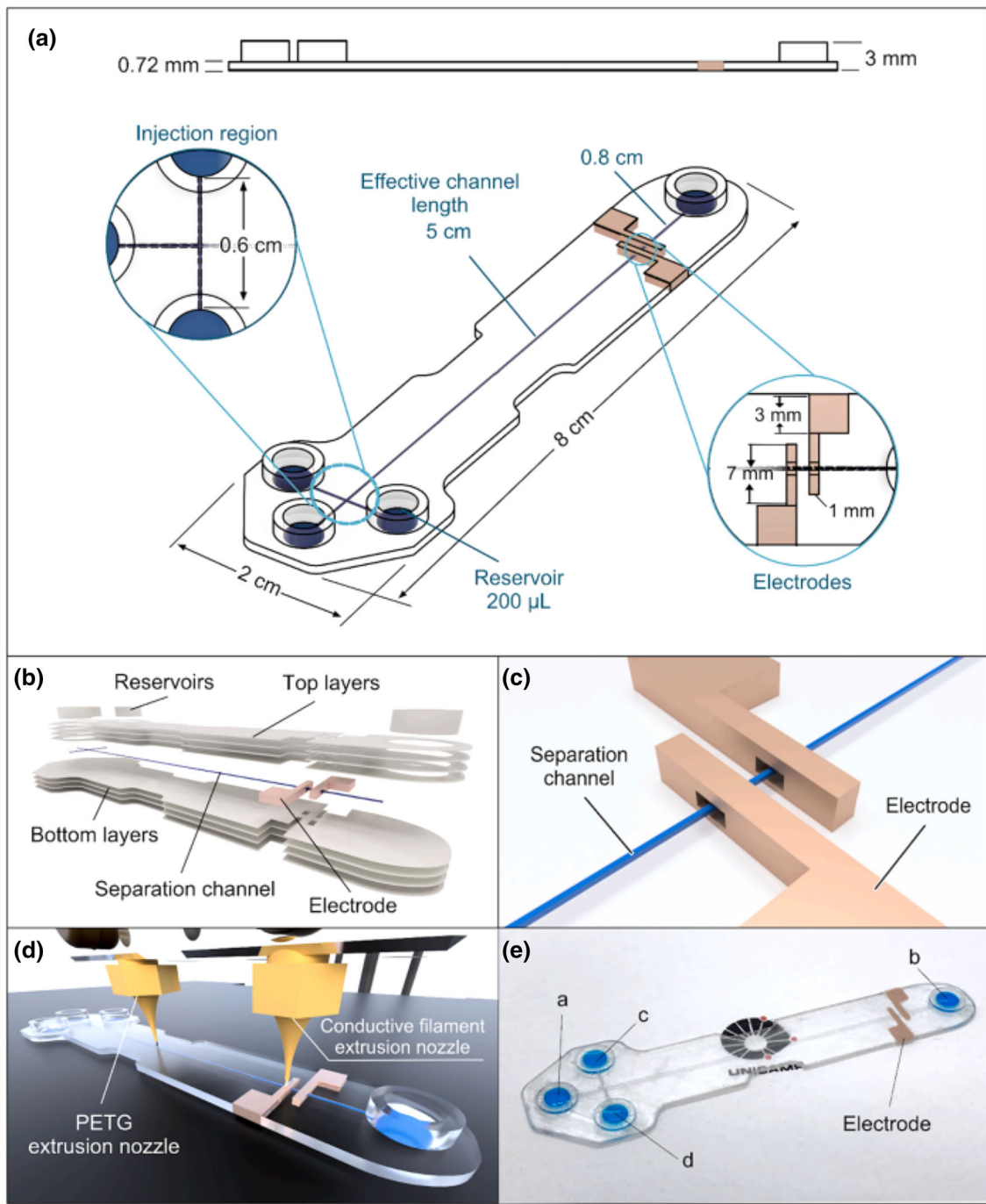


**Fig. 16** **a** Diagram showing the MCE-C4 D device along the dimensions of its 3D-fabricated parts; **b** magnified picture of the FDM 3D-fabricated layers; **c** Diagram showing the separating channel passing the 3D-fabricated electrodes, **d** two-extruding-nozzle 3D printing

process; **e** Actual picture of the MCE-C4D device, reservoirs containing blue dyes to improve visualization **a**, **b** for the BGE, **c** for the sample, and **d** for the auxiliary reservoirs [81]

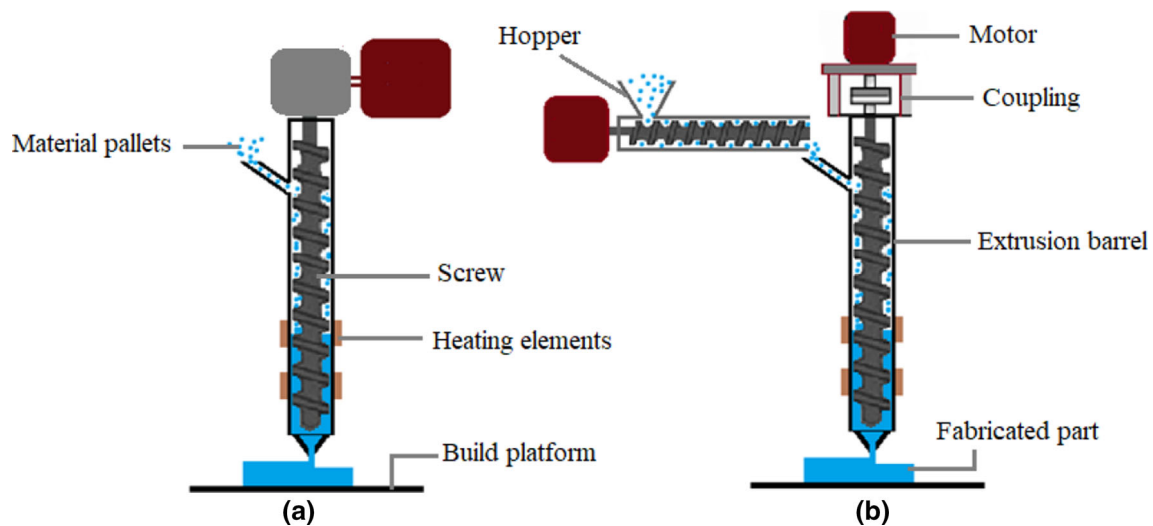


**Fig. 17** Schematic of pellet-based extrusion created by **a** Bellini [89]; **b** Reddy et al. [16]

resulting in increased flow speed. Also, chains of polymer move and glide quickly on one other as barrel temperature rises, causing increased material melt speed.

### 3.1 Small Volume Printing System

Figure 17 shows a schematic of two major small-volume printing systems developed. These systems can extrude directly from pellets and do not require material in filament form. Bellini used a heated barrel to contain an auger screw, whose extremities could fit deposition nozzles of various diameters [89]. The printing assembly could move in three dimensions while the printing surface was fixed [90]. The developed system was tested for printing temperature, material deposition velocity, and nozzle geometry for ceramic material. A significant finding was that there had been some agglomeration and air entrapped inside the deposited structures. This system was also utilized to make biopolymer scaffolds [91]. The printhead designed by [16] incorporated a distinct pellets feeder and a screw having changing channel depth and pitch to resolve the feeding difficulties reported by [90]. Many researchers developed their printers, and a minimum diameter of 7 mm was reported [92]. Another work for viscous polymer utilized infrared heating elements close to the printer's nozzle to avoid warping and delamination [93].

With time, various modifications were made to the fundamental design of the pellet-based screw-assisted extrusion system, and schematics are shown in Fig. 18. One such modification employed an auger screw [94]; they added four different loading holes at varying altitudes all along the barrel of the extruder to permit different material loading and improve process residency time control. For investigating

multi-material printing, fluorescent particles were incorporated into the melt. Another work [95] developed a screw of conical shape to produce greater plastic behavior and material homogeneity at a lesser length. Annoni et al. adapted a compact injection molding process with an inclined (at 45°) plasticating screw and a vertical piston-driven injection unit [96]. This arrangement enables extrusion process continuity and stability and a high extrusion force, allowing for the extrusion of very viscous fluids via a narrow nozzle exit diameter. To increase material flow management, Canessa et al. fitted a Moineau pump to the terminal of an auger screw [97]. The approach eliminates the requirement for retraction techniques by allowing discontinuous deposition even while the material is fed continuously. Khondoker & Sameoto created a twin-stage system consisting of a rigid horizontal plasticating unit coupled to a standard FFF deposition head [98]. This system solved the screw extruder's intrinsic constraints on its heaviness and inertia from the depositing head's pace and resolution demands.

A screw-assisted pellet extruder has been developed capable of extruding biopolymer mixtures such as polylactic acid (PLA) [99]. Additional functionality includes controlled pellet feeding, temperature control, and liquid cooling. The design of the pellet extruder includes the following parts;

**Hopper design:** feed the requisite amount of material and reduce conveying problems. A cylindrical hopper is used as the feeding issue is caused by the hopper corner in the square hopper. Generally, a hopper is gravity-assisted, but an agitator or stirrer can also be used for consistent pellet flow and to avoid material sticking.

**Drip feeder design:** for print quality to be consistent and avoid the extruder from jamming, control over the number of pellets to be fed is required. The feeder is placed just above the extruder, as shown in Fig. 19; the pellets were forced



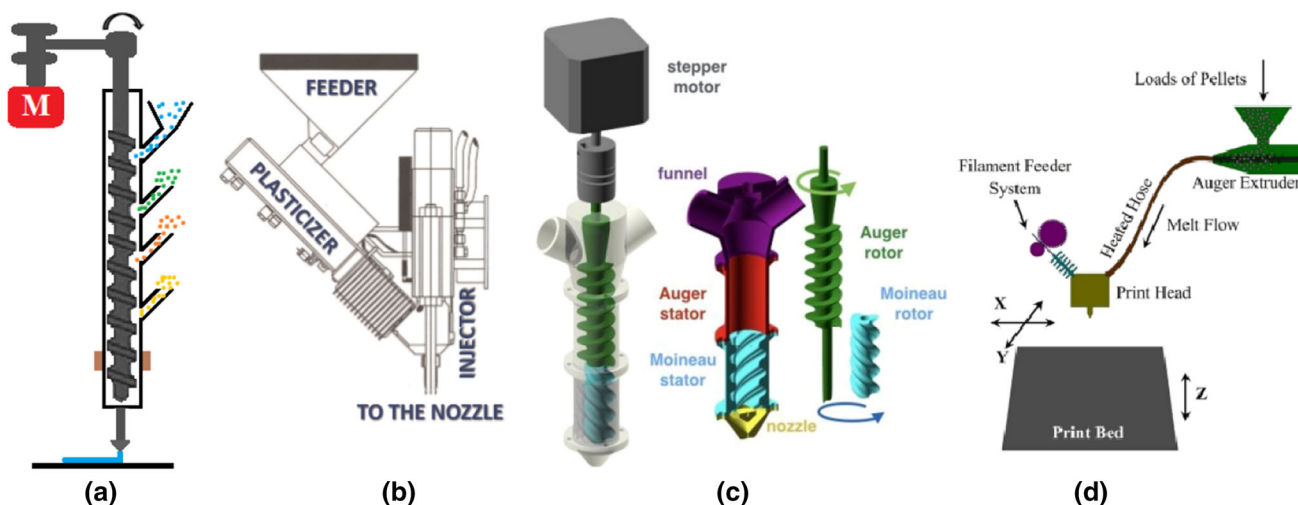


Fig. 18 Schematic of alternate designs of small-volume printing machines created by a Zhou et al. [94]; b Annoni et al. [96], c Canessa et al. [97]; d Khondoker and Sameoto [98]

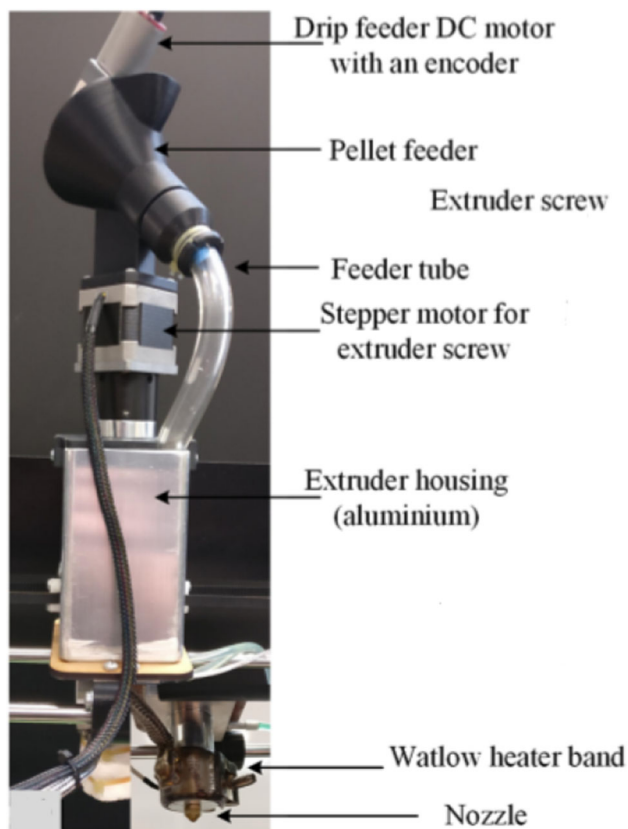


Fig. 19 Pellet extruder with built-in hopper and drip feeder [99]

out in low amounts at the desired pace by the extruder. The feeder’s form is comparable to the primary extruder shape to avoid edge effects and potential flow constraints.

Extruder screw design: it is the central part of the extruder, pellets are transported to the heating region using a screw, and the screw finally pushes the molten material and it comes out

of the nozzle. Variation of pressures across screw length is shown in Fig. 20.

Heating and cooling system: material undergoes shear and is used as a significant heating source in an extensive extrusion system. However, an externally powered electric heater was employed in this project. A closed-loop cooling arrangement with automotive-grade coolant was utilized to avoid pellets sticking on hot zones and blocking the extruder.

Variations in mechanical properties obtained for different extruder designs were minimal, showing significant reproducibility and consistency. Experiments confirmed that the strength obtained for printed parts is similar to the FFF process, and aesthetic quality is superior in their extruder because of uniform heating and cooling. This work has lots of scope for future work, like increasing the number of sensors used to supervise heating and cooling processes and precisely control the heat flow. Before the drip feeder activation, particular pressure is required and a pressure transducer can be used to check if that particular pressure is obtained.

Internal flow irregularities create detrimental impacts, including surging or spurt flow. Several other forms of variations in output products in screw extrusion operations are caused by external disruptions entering the operation from numerous sources [100]. Internal disruptions such as cyclic melt solid bed breakup and accumulation, flow contaminants, and nozzle flow abnormalities are additional well-known drivers of process variability. Another work considered an energy-based modeling method for screw-assisted pellet extruders used in 3D fabrication [101]. This modeling is associated with a balance of energy between the work done by the screw, the amount of heat energy lost by the nozzle heater, and the enthalpy of the extrudate. There are three zones on the extruder screw; a zone for transportation, a zone for melting, and a zone for mixing. The molten material is subjected

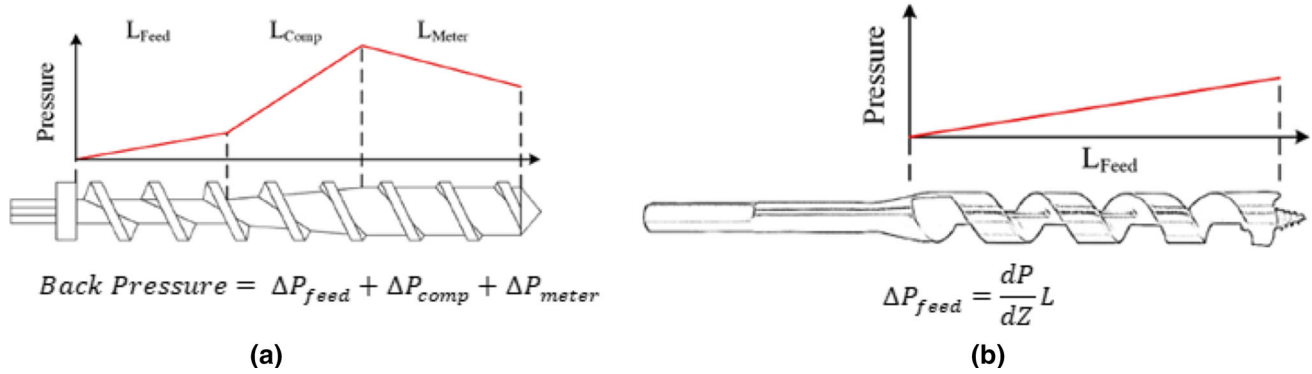


**Fig. 20** **a** Pressure profile of three-section screw; **b** pressure profile of auger drill bit [99]

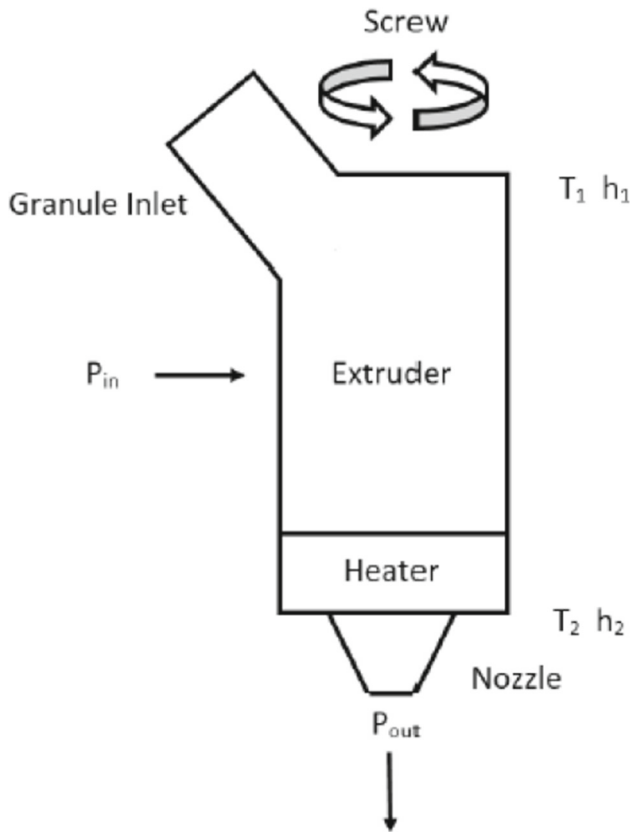


**Fig. 21** Screw extruder process [101]

to high pressure before dispensing through the nozzle. When the temperature at the screw inlet is too high than screw can melt the material even at the inlet and results in jamming the extruder. It also causes material burning and increases viscosity of material at outlet. Low temperature, on the other hand, restricts extrusion due to a slow melting rate, likely to result in jamming.

Specific enthalpy changes across stages 1 and 2 (Fig. 21) can be written as changes in enthalpy for forming (constant temperature) and melting (constant pressure) and are given

by Eqs. 9 and 10.

$$\Delta h = h_2 - h_1 = \Delta h_{\text{melt}} + \Delta h_{\text{form}} \quad (9)$$

$$\Delta h = \bar{C}_p(T_2 - T_1) + h_f + \frac{(P_2 - P_1)}{\rho} \quad (10)$$

$$P_{\text{out}} = \dot{m} \Delta h = \dot{m} \Delta h_{\text{melt}} = \dot{m} (\bar{C}_p(T_2 - T_1) + h_f) \quad (11)$$

Here  $P_1$  and  $P_2$  denote pressure at two stages,  $h_f$  is fusion-specific enthalpy, and  $\bar{C}_p$  is the average specific heat

Heat change can be written as

$$\Delta Q = \dot{Q} - \dot{Q}_{\text{losses}} = \frac{V^2}{R} + mfV_{\text{barrel}} \left( \frac{\pi DN}{H} \right)^{n+1} - \dot{Q}_{\text{losses}} \quad (12)$$

In Eq. 12,  $N$  is screw speed,  $m$  is consistency index,  $f$  is filling ratio,  $V_{\text{barrel}}$  is the Barrel's volume,  $D$  is the screw diameter, screw channel depth is  $H$ , the power-law index is  $n$ , the voltage at the heater is  $v$ , and the resistance of the heater is  $R$ .

$$P_{\text{losses}} - \dot{W} = \dot{Q} - P_{\text{out}} = \left( \frac{V^2}{R} + mfV_{\text{barrel}} \left( \frac{\pi DN}{H} \right)^{n+1} \right) - (\dot{m} (\bar{C}_p(T_2 - T_1) + h_f)) \quad (13)$$

The left-hand side of Eq. 13 is treated as a single measurement, and known values on the right-hand side can be used to find it. Two parameters control the system in this case,  $T_2$  and  $N$ . Experiment-derived values are  $V$  and  $\dot{m}$ . For distinctive  $T_2$  and  $N$  values,  $\dot{m}$  is measured. To find out the correlation between  $T_2$ ,  $N$  and  $\dot{m}$ , a search table is constructed.  $\dot{Q}$  and  $P_{\text{losses}} - \dot{W}$  are calculated by estimation at any fixed temperature and screw speed and temperature to determine  $P_{\text{out}}$ , and this is how  $\dot{m}$  is obtained. Pellets made of PLA having a low melting point can be used for 3D printing. Tests were performed with temperatures of 180 °C, 190 °C, and 200 °C. Screw rotational speeds were 1 RPS, 2 RPS, and 3 RPS; Fig. 22 illustrates their findings.

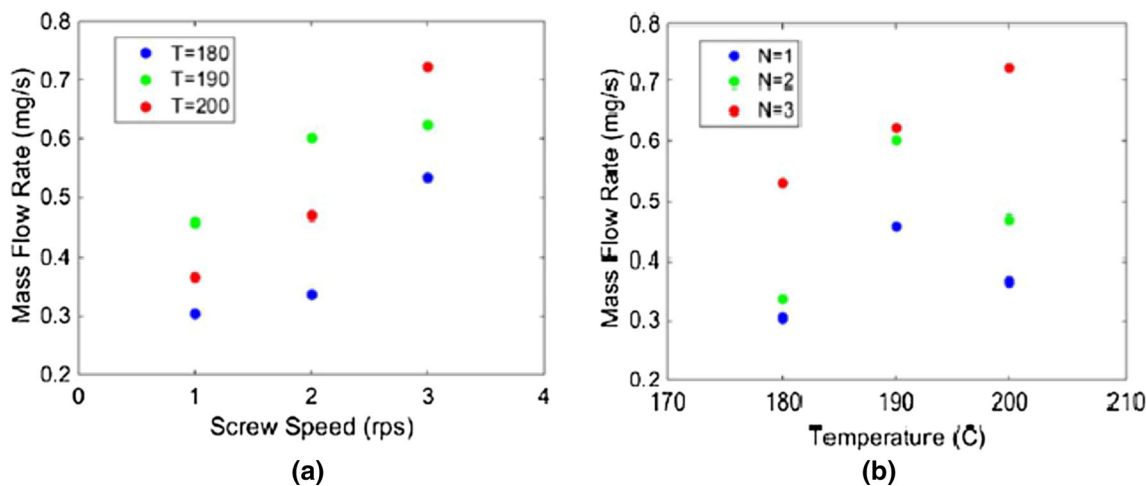


**Fig. 22** **a** Variation of mass flow rate with screw speed at various temperatures; **b** variation of mass flow rate with the temperature at various screw speeds [101]

The dynamic approach was modeled to use the experiments with steady-state data to fit a first-order dynamic model for mass flow concerning screw speed and temperature. Denoting  $\tilde{f}_t = \tilde{f}_t - \tilde{f}_{N, T_2}$  as mass flow rate variation from steady-state  $\tilde{f}_{N, T_2}$ . The mass of the extruded material can be written as shown in Eq. 14.

$$\begin{aligned}
 M_{t_{\text{final}}} &= \bar{f}N, T_2 t_{\text{final}} + \int_0^{t_{\text{final}}} \tilde{f}_t d\tau \\
 &= \bar{f}N, T_2 t_{\text{final}} + \frac{\tilde{f}_0}{k} (1 - e^{-k t_{\text{final}}}) \\
 &\quad + \frac{\alpha T_2}{k} (t_{\text{final}} - t_{\text{switch}}) - \frac{\alpha \tilde{T}_2}{k^2} (1 - e^{-k(t_{\text{final}} - t_{\text{switch}})})
 \end{aligned}
 \tag{14}$$

Constants  $\alpha$  and  $k$  used in Eq. 23 are obtained by experiments.

Using the data validation helps look for active controllers of extruders using known extrusion rates.

A conveyor worm is modeled in 3D to create a new extruder to reduce the cost of manufacturing compared to traditional 3D extruders [102]. Raw material for the new extruder is ABS or PLA or any new materials later developed. AutoCAD was used to design a 3D model of a screw used in an extruder by moving a cone trunk, as shown in Fig. 23a, having variable dimensions after a conical worm wound on a cone whose axis of symmetry coincides with the axis of the axis symmetry of the worm. To define the trunk cone axis, vector calculations were used. Auto-Lisp is used for calculating the points belonging to a propeller and represented in AutoCAD and then transported to inventor, where the snail was finally modeled. It was then exported in “STL” format, and printing was done in a 3D printer; finally, the casting mold was executed and poured.

In Fig. 23a, a conical propeller is shown where  $r$  is the small base radius of the cone trunk,  $p$  is the propeller step, and  $\beta$  is the inclination angle of the generator cone trunk with the OZ axis.

Using AutoCAD command circle and extrude, a cylinder is represented, a cone on which a conical propeller is wrapped associates fixed coordinate system (S) and a mobile coordinate move (S1) along with a conical propeller (Fig. 23b). For obtaining the coordinate of point  $P_2$  vector  $\overrightarrow{P_1 P_2}$  which depends upon the coordinate of point P1 (0, 0,  $z_{p1}$ ) and  $P(x, y, z)$ . Based on  $O(0, 0, 0)$ , the coordinates of point  $P_2$  can be determined.

The actual model obtained is shown in Fig. 23c. This work helps simplify the modeling of the worm, which helps in 3D printing and checking how the model works at reduced cost in less time. Deprivation is that finishing with numeric control after casting is difficult in manufactured 3D modeling worms, which can be overcome by using a cylinder representing frontal-cylindrical milling tool.

Manideep et al. developed a screw-based pellet extruder from basic concepts of 3D printing. This extruder reduces the cost of manufacturing to almost half the cost compared to filament or wire type of extruder and to use as a multi-functional extruder. The single-screw extrusion system is shown in Fig. 24. In any pellet-based 3D printer, an extruder is a prime component that feeds the pellets to the heat exchanger region—a horizontal extruder consisting of a heat exchanger, motor, and a guiding system. The thermoplastic material typically used is acrylonitrile butadiene styrene (ABS), with a melting point of 200°. To withstand high temperatures, steel F-174 was used as an extruder material. A 6-mm-diameter screw was used, having a screw length of 300 mm. Total length is divided into three regions feeding zone of a length

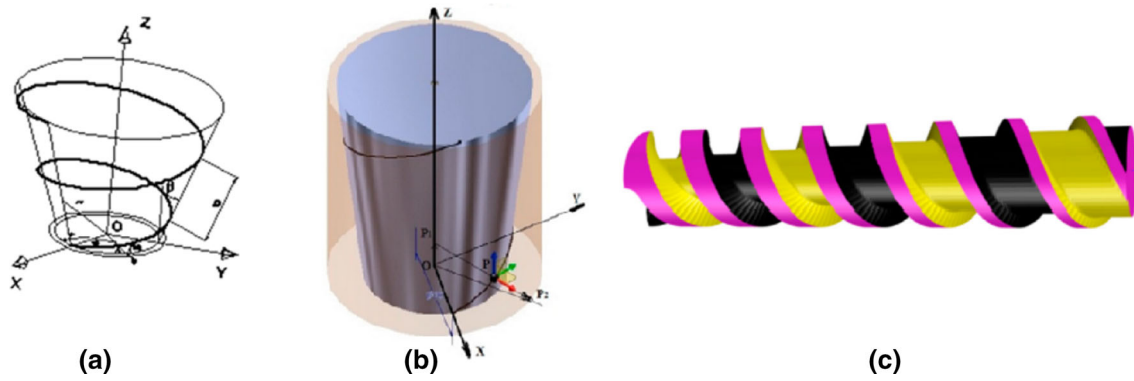
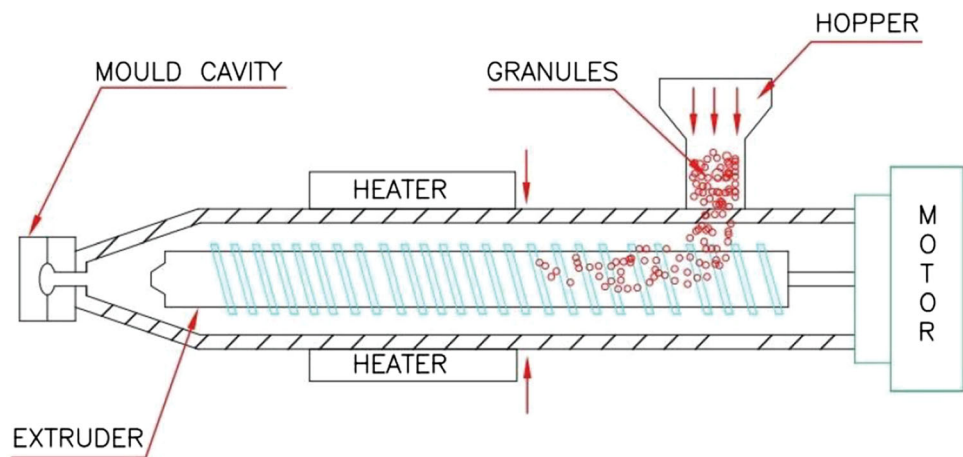


**Fig. 23** a Conical propeller; b associated coordinate system; c 3D model obtained [102]

**Fig. 24** Single screw extrusion system [1]



of 31.45 mm, a compression zone of 51.45 mm, and a metering zone length of 63.075 mm.

Significant components of the developed extruder are: nozzle: brass is used as material as it has good characteristics for a more extended period. Hopper: to feed the pellets to the heat exchanger region. Heat exchanger: the temperature of the heat exchanger depends upon the material to be extruded; for ABS, it is about 270°. Horizontal guiding system: developed pellet extruder is a horizontally designed extrusion unit with a horizontally arranged heating system, motor, and extruder.

Volumetric flow rate ( $Q$ ) depends on three types of flow: the drag flow induced by the screw turning, the pressure flow that restricts the system flow, and the filtration flow caused by the material loss in the screw cylinder clearance.  $Q$  is expressed by Eq. 15.

$$Q = \left( \frac{\alpha K}{K + \beta + \gamma} \right) \eta \quad (15)$$

where the drag flow coefficient is  $\alpha$ ,  $K$  is constant for the geometrical head, the pressure flow coefficient is  $\beta$ , the filtration flow coefficient is  $\gamma$ , and the spindle speed is  $\eta$ . The power required to melt the plastic can be calculated based on

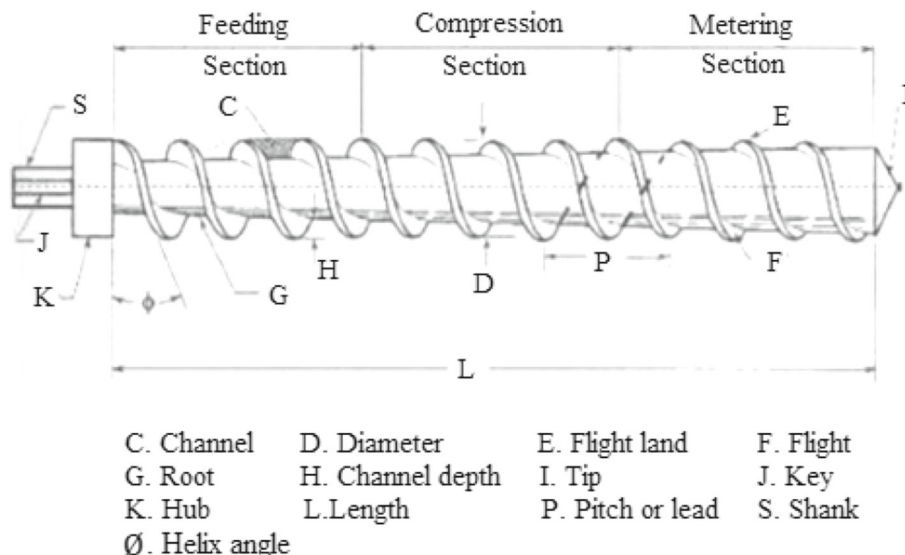
the volume flow rate. By using this extruder, it was observed that cost of printing for 1.75 mm plastic wire at the rate of 0.4 kg/h and specific power consumption of 0.24 kWh/kg was INR 320 per kg, whereas conventional printing for the same material costs INR 1246 per kg [1], and hence this extruder reduces the cost of printing considerably.

The work carried out by Wankhade et al. [103] aims to create a portable 3D printing filament-making machine that can draw ABS filament cheaply. The components of this unit are: screw: it should be challenging and bear high temperatures; for this purpose, steel F-174 is used in nitriding steel.

The geometry of the screw is shown in Fig. 25. A 25-mm-diameter screw is used, and a 300 mm length is considered to keep it lightweight. No. Of channel is 1, screw angle  $\varnothing = 17.65^\circ$ , ridge width is  $e = 0.12 \times D = 3$  mm. Screw lengths are feeding zone 20–25%, 65 mm, compression zone 32–38%, 105 mm, metering zone 40–45%, 130 mm. Channel depth  $H = 0.2 \times D = 5$  mm, fillet clearance  $\delta = 0.002 \times D = 0.05$  mm, the barrel's diameter is calculated by the sum of screw diameter and fillet clearance = 25.05 mm.

Nozzle: to withstand high temperatures 2 mm brass plug was used.

Fig. 25 Screw geometry [103]



Hopper: for the gravity feed hopper, stainless steel was used.

Motor: 55 RPM motor with 61 kg-cm torque was connected by PWM (Pulse Width Modulation) controller.

Heating systems: 35 × 30 mm 150-Watt heating band was used.

Fixing system: Square shaped mild steel tube was used.

The extruder’s main component is a barrel with a screw attached to a heater at the far end. An electric motor drives the screw, conveying the resin pellets through the barrel to the heater by mechanical action. Pellets absorb heat from heating elements, become soft, and melt, finally extruded through a die.

Janssen’s assumption can determine stress in the hopper as in Eq. 16.

$$\sigma = K \times P_v \tag{16}$$

Normal compressive stress  $P_v$  can be determined by Eq. 17.

$$P_v = \frac{\rho g D}{4\mu K g_c} \left( 1 - \exp\left(-\frac{4z\mu K}{D}\right) \right) \tag{17}$$

where  $g_c$  = gravity conversion constant, density is  $\rho$ , Janssen constant is  $K$ ,  $\mu$  is the coefficient of wall friction. The motor is continuously driving screw, so pellets are pushed toward the heater, and the ABS filament gets soft and melt. The filament of die diameter was obtained as it was pushed through a die. The air fan cools the heated filament coming from the die. Screw extrusion allows access to a wide variety of materials for 3D printing.

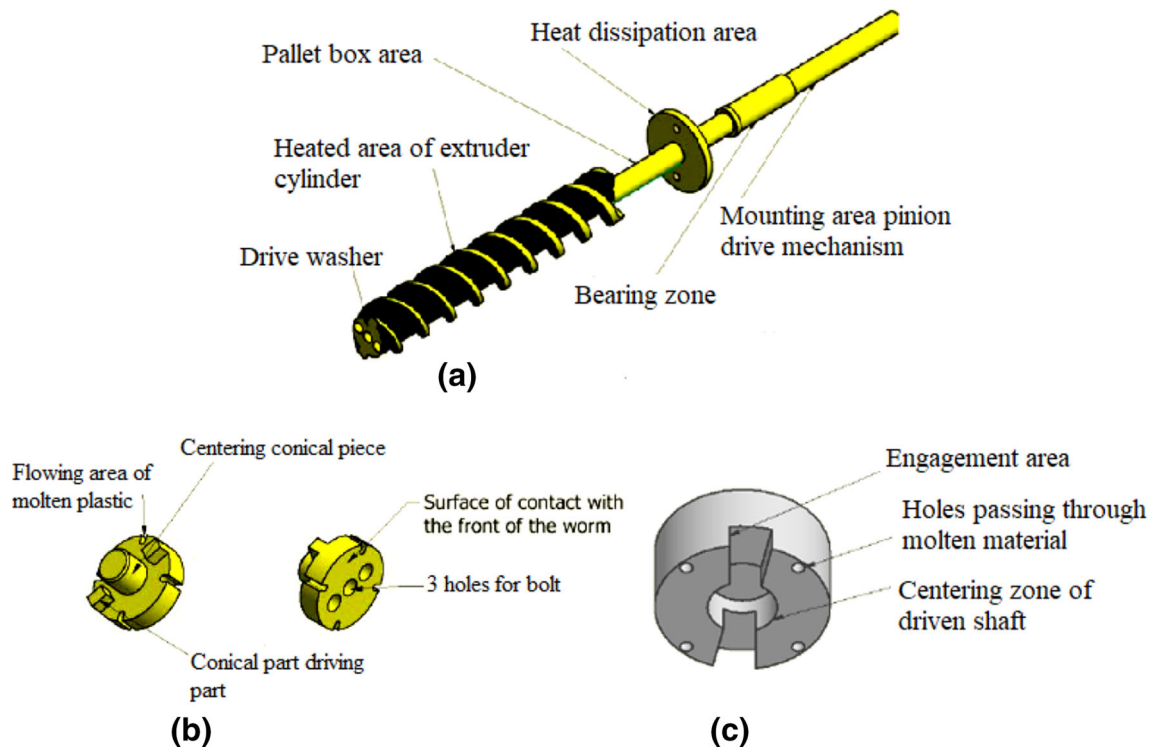
The filament-based 3D printing could not print the part of flexible material. The material with certain rigidity could be used as filament, which limits the material scope of the fused

Table 4 Cost of raw material [107]

Raw material	Company	Price (lei/kg)
ABS filament	Optimus digital	79.39
ABS pellets	Romcarbon Sa	4.34
Difference in price		75.5

filament fabrication process. Material such as PEEK, with high viscosity and melting temperature, could not produce stable flowability at high printing speed. Hence, Tseng et al. [93] developed a screw extrusion-based additive manufacturing system to print the parts with PEEK material. 96% of the bulk material strength is present in the pieces produced by the screw extrusion technique, which exhibit constant mechanical characteristics. By maintaining the nozzle temperature between 370 and 390 °C and the build plate temperature up to 280 °C, they were able to maintain the extrusion rate of 1.5 g/min. Their observations using SEM and XRD reveals that mechanical properties are highly affected by the thermal conditions and the post-annealing process does not play any significant role in varying the material properties. Moreover, controlled material extrusion is one of the major problems in screw extrusion-based additive manufacturing systems [104, 105]. For printing a dimensionally correct object with a pellet-based extruder, the extruder must position itself without depositing the material during repositioning [99, 100]. This work was carried out mainly to overcome this problem by providing a continuous supply of material during printing and reversal of melt into the extruder of printer operation with pellets of ABS [107]. The need to develop the pellet extruder is justified by the cost difference between filament and pellet shown in Table 4. A conical conveyor worm is selected for the continuous material flow, as shown in Fig. 26a. In the





**Fig. 26** **a** Conveyor worm; **b** drive washer; **c** tapered piece [107]

front, three holes are provided for fixing the drive washer, the area for transporting pellets, pellet feeding, heat dissipation zone, bearing attachment zone, and the area for attachment with an electric motor (Table 5).

Two-piece assemblies were used to ensure the retraction of material, drive washer, and tapered piece. This assembly ensures the blockage of material at certain times. As shown in Fig. 26b, the drive washer is attached to a screw by three bolts; it has recesses on the circumference to allow a flow of molten material, a cylinder for centering, and two diametrically opposite located engagement zones. Fluid material penetration into the flow area through holes in the tapered piece depends upon the screw rotation direction. Four holes were designed on tapered pieces (Fig. 26c) for material flow; when the screw rotates in the feed direction, it continues in the recess in the driver shaft. Whenever the screw rotates in the reverse direction, the conical piece does not continue in the drive washer recess.

In the reverse direction of the feed screw, the friction coefficient between the conical piece and the drive washer is lower than the friction coefficient between the bearing and conical piece; hence, vacuum is formed, and the issue of molten material retrieval is solved. Optimized process parameters play an important role in printing a part with desired dimensional accuracy, mechanical strength, and surface quality [102, 103]. Several attempts were made to print ABS pellets with different parameters. Changing the direction of screw

retraction was not controlled, and the material continued to flow. Inside the extruder, too high pressure is developed, the conical piece is pushed by molten material, and a space is created between the conical piece and the drive washer.

### 3.2 Large Volume Printing System

Large-volume printing utilizing a pellet-based screw-assisted system has almost the same functional operation as the vertical screw system, as shown in Fig. 27. Some have auger screws or standard extrusion screws featuring compression profiles, while others have customized depositing heads. Robotic arms were used more frequently in experimental models than Cartesian platforms. Hertle et al. used a gantry structure with a screw-assisted welding extruder and a deposition surface that moves in two directions [110]. The device was designed to analyze material adherence in shear test specimens and loaded using polymer pellets. Magnoni et al. combined a benchtop-sized screw extruder with a six-axis robotic arm to create large-volume 3D printing using polymer granules [111]. Their research focused on estimating process parameters' impact mainly on the substrate material's width and height. Brooks et al. developed a screw-driven deposition technique that may be utilized for 3D printing of large volumes [112]. This technique was examined to produce parts with thin shells, and no supports were used. This system does not have the movement of the printhead; instead, the robotic



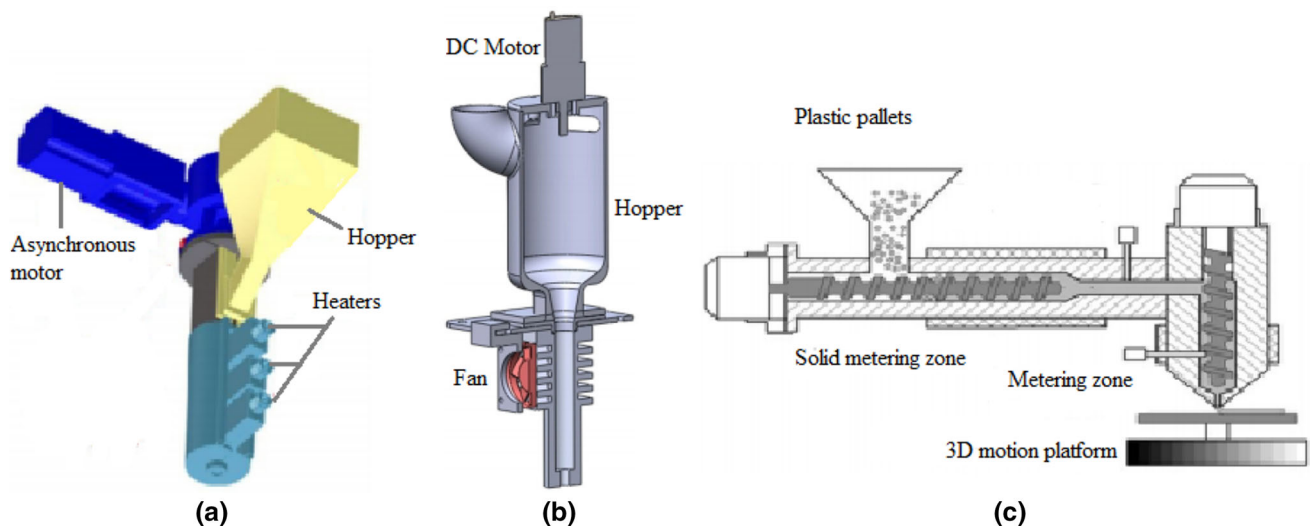


**Fig. 27** Schematic of large-volume printing extruders created by **a** Magnoni et al. [111]; **b** Brooks et al. [112]; **c** Liu et al. [113]

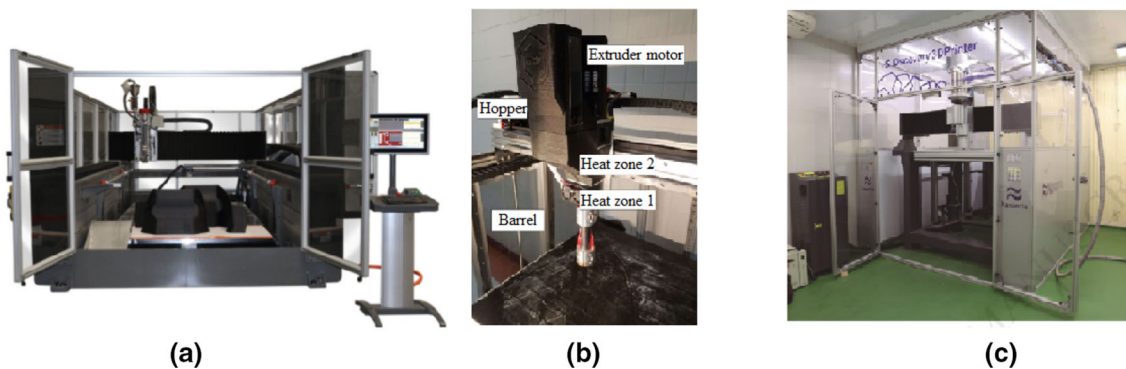


**Fig. 28** Screw-assisted large volume pellet-based 3D printer **a** BAAM®; **b** Gigabot X® [86]; **c** Discovery 3D Printer® [87]

arm was fitted with a convex depositing surface that allowed it to move with six degrees of freedom. Liu et al. developed a two-stage extruder system; a screw having a compression profile accounts for delivering and melting the material granules during the first stage, whereas an auger screw regulates the amount of material to be extruded during the next stage [113]. Each screw can also be moved individually, as well as the vertical screw can spin backward throughout the 3D printing process to retract the material.

Commercial large-volume printing machines are BAAM® 3D printer, Gigabot X® 3D printer, and Super Discovery 3D Printer®; these machines are shown in Fig. 28. The BAAM® machine's printhead travels along the *x*-axis, and the build platform travels along the *y*-axis and *z*-axis. For Super Discovery 3D Printer® and Gigabot X®, the printhead travels in the *x*-axis and *y*-axis, while the build platform movement is along the *z*-axis.

The evolution of the BAAM® system was disclosed by [114]. BAAM machine is 10 times larger, 20 times cheaper, and 200 times faster than traditional material extrusion AM

systems. This system can deposit clean ABS having stiffness equivalent to injection molded polymers and can do so regardless of depositing direction. A reciprocating *z*-tamping component was fitted to the print head to minimize porosity and increase interfacial adherence. The technology's viability was first shown using pure polymer granules, but fiber-reinforced polymers were favored due to more significant warping and distortion. The fiber reinforcement can greatly enhance stiffness and strength in the principal depositing direction. The BAAM system was used to deposit a wide variety of polymers, demonstrating that it can print composite materials having high strength (above 60 MPa) and stiffness (above 12 GPa), but substantial anisotropy is introduced.

Woern et al. [86] used a range of granular materials, comprising pure pellets and recycled materials, to evaluate the performance of the Gigabot X® 3D printer. An investigational grid was devised to find the best printing variables for every polymer concerning depositing speed and temperature. Results revealed that material particle shape greatly

**Table 5** Comparison between the filament and pellet-based 3D printers [63, 99, 106, 108, 109, 115–125]

	Filament printer	Pellet based printer
Material cost	High cost involved in producing filaments	Low as there is no need for turning pellets into filaments
Choice of material	Limited as processing a few pellets into filaments is challenging	A wide variety, even the brittle polymers which are challenging to spool can be used
Printing speed and build size	Low as most printers use filaments of 1.75 mm diameter	High as just screw speed and size can affect how much flow a pellet extruder can produce
Resolution	High since a small nozzle is used fine tolerances and intricate geometries can be printed	Low as using larger nozzles results in lower resolution, and high tolerances
Flow control	Smooth as the rate of flow of filament may be predicted analytically with ease	Complex extruding system
Thermal management	Use of small nozzle results in better interlaminar adhesion	The use of a large nozzle may cause one layer to cool and solidify insufficiently to hold the following layer
Bulkiness	Lightweight and occupy less space	Relatively bulky and space-consuming

influences the depositing speed. The tensile strengths of components produced by typical FFF/FDM and Gigabot X<sup>®</sup> 3D printers are equivalent to all tested materials. That implies that by using this printer; there is no sacrifice in part strength.

Nieto et al. put the Super Discovery 3D Printer<sup>®</sup> to the testing to see if it might be used in the marine sector [87]. The printhead had a flexible arm that could be attached to various instruments, including a surveillance camera to control the 3D fabrication process from a distance. A multi-variable approach was used to represent the selection of material and process of validation, which aided decision-making when choosing material for a screw-assisted large-volume pellet-based extrusion process. Thermomechanical deformations, extrusion variables, and processing behaviors all played a role in this process. Two polymers (PLA 3D850 and fire-resistant ABS TOYOLAC) met the criteria for being extruded

and processed by a screw-assisted large-volume pellet-based machine for extended periods. Few clean materials showed significant heat deformation, while the fiber-reinforced composite materials had inadequate printability. It should be mentioned that the fibers and polymer granules were manually blended and not adequately compounded in this investigation; as a result, nozzle clogging could have been caused.

## 4 Discussion

Numerous advancements have been made in extrusion-based AM over time; still, some challenges are overcome for improved printing quality. In the earlier work, the liquefier was redesigned to be straight from curved. This modification reduced the extrusion force by 150%. The revised design with various deposition head materials made 3D printing of metallic components easier by utilizing greater strength alloys. A customized pressure transducer and a thermocouple are designed to assess the produced melt temperature to overcome the inability to provide relevant real-time data. An in-line FDM rheometer measures viscosity accurately for a broad range of temperatures and shear rates. Filament breakage is among the most common FDM process faults, and it can result in nozzle clogs, geometrical dislocations, and manufacturing failure. Depending upon the process parameters, a critical feed rate is determined. Now acoustic emission (AE) approach can be used. It was determined from the FDM process that the probability distribution of broken AE signals differs, which can be demonstrated by the use of two quantifiable indexes, instantaneous skewness, and relative similarity. It is possible to use instantaneous skewness as an initial indicator for filament breaking. However, filament breaking can be comprehensively identified by relative similarity. Another significant process error in FDM is nozzle clogging. The printed parts' consistency is adversely affected by surface roughness, geometric tolerance, or mechanical properties. The condition of the nozzle can be assessed by the accelerometer, which measures the vibration of the mounting bar that supports liquefier assembly for both the Bowden and Direct extruder. Additive manufacturing of metals requires electron or laser beam concentrated heating and solidification of metal powder. These methods are costly as they require intensive energy sources, control of the atmosphere, grain control of powder, and post-processing for dimensional accuracy. A printing force ranging from 10 to 1000 N is ideal for practical reasons; printing forces of more than 1000 N are challenging and costly in 3D printing, but forces less than 10 N become particularly tedious to regulate. Bulk metallic glasses (BMGs) exhibit such behavior, mainly when depositing through a 0.5-mm aperture, the viscosity should be below  $10^6$  Pa s, and when depositing via a 2-mm aperture, the viscosity should be below  $10^8$  Pas.

Most traditional 3D printer uses only a single-color filament which limits the use of 3D printing, one way to overcome this is to carry out different color mixing. The filament's flow condition is complicated, and temperature field control is vital in color print mixing. Using a single-nozzle extruder for multi-color/material printing necessitates additional time for filament change and nozzle clean-up, making the printing process complex and time-consuming. Hence, multiple-color printing is another way to use a multi-nozzle extrusion system. Only two stepper motors were used on a multi-nozzle extruder in a model, allowing for concurrent printing of five distinct colors and materials. Furthermore, the extruder hot end is powered by just two stepper motors, reducing the extra size and heaviness of the hot end while also increasing printing speed. The Bowden-type extruder is preferred in such systems because the operating parts and the hot end are segregated.

Pellet-based extrusion 3D printers do not require material to be available in the filament form; instead, granules are used. This allows pellet-based extruders to be used to print biopolymers and high-carbon fiber materials. Using proper heating and cooling systems, this extruder can produce components with a strength similar to the FFF process and superior aesthetic quality. Internal flow irregularities create detrimental impacts, including surging or spurt flow. Internal disruptions such as cyclic melt solid bed breakup and accumulation, flow contaminants, and nozzle flow abnormalities are additional well-known drivers of process variability. The extrusion rate is the manipulated variable in this extrusion process. An energy-based modeling approach for screw-assisted pellet extruders can be used in 3D fabrication. This modeling is associated with a balance of energy between the work done by the screw, the amount of heat energy lost by the nozzle heater, and the enthalpy of the extrudate. The temperature profile across the extruder is monitored using an arrangement of thermistors for feedback. The speed of the screw can be set for a stepping motor that transports the material. A dynamic model was constructed on top of a steady-state model for a controller that can accurately control flow based on the estimation of the extrusion rate.

Pellet extruders reduce the cost of 3D manufacturing to almost half the cost compared to filament or wire types of extruders. The horizontal extrusion process in which one side of the auger bit is attached to the heating system, preceded by a hopper for retaining pellets as they move into the heating unit, and the other side is attached to the electrically driven motor that drives the whole extrusion system. When examining the pricing of the pellet extruder, consider the 1.75 mm plastic filament utilized in a traditional filament-based 3D printer costing INR. 1246 for 1 kg. A Pellet extruder employs pellets of the material, the same as used in a filament-based 3D printer, which costs INR. 320 for 1 kg [1]. For printing a dimensionally correct object with a pellet-based extruder,

the extruder must position itself without depositing the material during repositioning. Two-piece assemblies ensure the retraction of material, namely tapered pieces and drive washers. This assembly ensures the blockage of material at certain times. Given the high pressures created within the extruder, the conical part is driven by molten material, and a gap is generated between the driving washer and the conical part. The molten material keeps flowing even when the worm's rotation direction changes; hence the retraction is not regulated. If productive alterations are implemented, the intended extruder could be used on 3D printers.

## 5 Conclusions and Future Trends

Extrusion-based additive manufacturing uses two types of technologies: filament extrusion and pellet extrusion. Different researchers studied these processes in detail and found that filament allows for finer detail, close tolerances, and precise control over the material flow rate. At the same time, reduced prices and increased material domain in pellet-based extruders unlock plenty of new possibilities for 3D printing. Extrusion-based additive manufacturing is the most frequent and perhaps the most straightforward method of 3D printing, but it involves complexities during printing. This paper covers a detailed study of 3D printing process complexities, including filament breakage, nozzle clogging, in-line rheological monitoring, multi-color printing, and material retraction. 3D printing capabilities were upgraded, and limitations were addressed by altering components or providing more functions. The significant findings of this review work are concluded below.

- Tensile strength, compressive strength, yield strength, flexural strength, hardness, ductility, dimensional stability, surface finish, and manufacturing time are all affected by distinct process parameters.
- Nozzle temperature is among the most significant process variables that directly impact the mechanical properties of printed components.
- Another major issue in EB-AM is nozzle clogging. Nozzle clogging occurs for various reasons, including dust within the liquefier, the lack of extrusion space due to inadequate layer thickness, or the distortions of the printed component. Lowering the temperature of the nozzle solidifies the filament at the nozzle's inner side, this causes a reduction in the diameter of the filament, and it is employed as a technique simulating for clogging of the nozzle during extrusion.
- The use of numerous sensors for monitoring FDM is critical for understanding technology and establishing control mechanisms for the production process. The acoustic



emission technique is used for monitoring filament breakage, and this technique has the advantage that it can detect bursting and weak signals even from complex backgrounds.

- Filament extruder handles oozing and retraction easily, and there is only one heat region to monitor, and slight modifications in flow rates are required for new material compared to multiple heat regions in a pellet extruder. The tightly regulated, rapidly varying flow rate behavior necessary for a 3D printer is difficult to achieve with a screw.

Nowadays, the industry is shifting toward pellet-based extrusion 3D printers, especially for high carbon fiber materials, which are frequently used to minimize warpage and boost strength. This paper also describes a pellet-based extruder's development and design for extruding biopolymers such as PLA. Vertical screw-assisted extruders are the most widely used positive alternative, into which material pellets are supplied and then dispensed by the nozzle in a single-stage process. The conglomeration condition of the pellets appears to be more important than the physical characteristics of the feedstock material in an effective extrusion process, and changes to the screw design were made mainly to satisfy particular performance standards. The printheads for a small-volume printing system require an extensive mechanism of the miniaturized screw, and its manufacture may account for the majority of the expenditures. Benchtop-sized screw extruders can help large-volume printing systems conserve money and time by decreasing expenses and speeding up machine development. To utilize the strengths and weaknesses of filament and pellet-based extrusion processes, the present review work can be utilized to develop a multi-material hybrid form of a 3D printer in the future, capable of printing both filaments and pellet forms of materials on the same setup.

**Acknowledgements** This work was supported by the Science and Engineering Research Board (SERB)–DST, New Delhi, India, under its Start-up Research Grant (SRG) scheme [Grant Number: SRG/2019/000943].

## References

1. Manideep, P.; Subbaratnam, B.; Harsha, M.: Design and development of pallet extruder. *AIP Conf. Proc.* (2019). <https://doi.org/10.1063/1.5141260>
2. Vaezi, M.; Chianrabutra, S.; Mellor, B.; Yang, S.: Multiple material additive manufacturing—part 1: a review: this review paper covers a decade of research on multiple material additive manufacturing technologies which can produce complex geometry parts with different materials. *Virtual Phys. Prototyp.* **8**(1), 19–50 (2013). <https://doi.org/10.1080/17452759.2013.778175>
3. Patel, A.; Taufik, M.: Stage dependent strengthening of fused filament fabricated components. *Mater. Today Proc.* **50**, 1853–1861 (2021). <https://doi.org/10.1016/j.matpr.2021.09.231>
4. Joshi, S.C.; Sheikh, A.A.: 3D printing in aerospace and its long-term sustainability. *Virtual Phys. Prototyp.* **10**(4), 175–185 (2015). <https://doi.org/10.1080/17452759.2015.1111519>
5. Segonds, F.: Design by additive manufacturing: an application in aeronautics and defence. *Virtual Phys. Prototyp.* **13**(4), 237–245 (2018). <https://doi.org/10.1080/17452759.2018.1498660>
6. Leal, R., et al.: Additive manufacturing tooling for the automotive industry. *Int. J. Adv. Manuf. Technol.* **92**(5–8), 1671–1676 (2017). <https://doi.org/10.1007/s00170-017-0239-8>
7. Francis, M.P.; Kemper, N.; Maghdouri-White, Y.; Thayer, N.: *Additive Manufacturing for Biofabricated Medical Device Applications*. Elsevier, Amsterdam (2018)
8. Yap, Y.L.; Yeong, W.Y.: Additive manufacture of fashion and jewellery products: a mini review: this paper provides an insight into the future of 3D printing industries for fashion and jewellery products. *Virtual Phys. Prototyp.* **9**(3), 195–201 (2014). <https://doi.org/10.1080/17452759.2014.938993>
9. Sutton, A.T.; Kriewall, C.S.; Leu, M.C.; Newkirk, J.W.: Powder characterisation techniques and effects of powder characteristics on part properties in powder-bed fusion processes. *Virtual Phys. Prototyp.* **12**(1), 3–29 (2017). <https://doi.org/10.1080/17452759.2016.1250605>
10. Taufik, M.; Jain, P.K.: Role of build orientation in layered manufacturing: a review. *Int. J. Manuf. Technol. Manag.* **27**(1/2/3), 47–73 (2013)
11. Tamburrino, F.; Barone, S.; Paoli, A.; Razionale, A.V.: Post-processing treatments to enhance additively manufactured polymeric parts: a review. *Virtual Phys. Prototyp.* **16**(2), 218–251 (2021). <https://doi.org/10.1080/17452759.2021.1917039>
12. Siddaway, A.P.; Wood, A.M.; Hedges, L.V.: How to do a systematic review: a best practice guide for conducting and reporting narrative reviews, meta-analyses, and meta-syntheses. *Annu. Rev. Psychol.* **70**(1), 747–770 (2018). <https://doi.org/10.1146/annurev-psych-010418-102803>
13. Turner, B.N.; Strong, R.; Gold, S.A.: A review of melt extrusion additive manufacturing processes: I. Process design and modeling. *Rapid Prototyp. J.* **20**(3), 192–204 (2014). <https://doi.org/10.1108/RPJ-01-2013-0012>
14. Mohan, N.; Senthil, P.; Vinodh, S.; Jayanth, N.: A review on composite materials and process parameters optimisation for the fused deposition modelling process. *Virtual Phys. Prototyp.* (2017). <https://doi.org/10.1080/17452759.2016.1274490>
15. Patel, A.; Taufik, M.: Advances in nanocomposite material for fused filament fabrication. *Polym.-Plast. Technol. Mater.* (2022). <https://doi.org/10.1080/25740881.2022.2072225>
16. Reddy, B.V.; Reddy, N.V.; Ghosh, A.: Fused deposition modelling using direct extrusion. *Virtual Phys. Prototyp.* **2**(1), 51–60 (2007). <https://doi.org/10.1080/17452750701336486>
17. Comelli, C.A.; Davies, R.; van der Pol, H.J.; Ghita, O.: PEEK filament characteristics before and after extrusion within fused filament fabrication process. *J. Mater. Sci.* **57**(1), 766–788 (2022). <https://doi.org/10.1007/s10853-021-06652-0>
18. Singh, M., et al.: Additive manufacturing of mechanically isotropic thin films and membranes via microextrusion 3D printing of polymer solutions. *ACS Appl. Mater. Interfaces* **11**(6), 6652–6661 (2019). <https://doi.org/10.1021/acsami.8b22164>
19. Diouf-Lewis, A., et al.: Design and characterization of carbon fiber-reinforced PEEK/PEI blends for fused filament fabrication additive manufacturing. *Mater. Today Commun.* (2022). <https://doi.org/10.1016/j.mtcomm.2022.103445>
20. Rajakaruna, R.A.D.N.V.; Subeshan, B.; Asmatulu, E.: Fabrication of hydrophobic PLA filaments for additive manufacturing. *J. Mater. Sci.* **57**(19), 8987–9001 (2022). <https://doi.org/10.1007/s10853-022-07217-5>
21. Garmabi, M.M.; Shahi, P.; Tjong, J.; Sain, M.: 3D printing of polyphenylene sulfide for functional lightweight automotive





- component manufacturing through enhancing interlayer bonding. *Addit. Manuf.* **56**, 102780 (2022). <https://doi.org/10.1016/j.addma.2022.102780>
22. Das, A., et al.: Current understanding and challenges in high temperature additive manufacturing of engineering thermoplastic polymers. *Addit. Manuf.* **34**, 101218 (2020). <https://doi.org/10.1016/j.addma.2020.101218>
  23. Xiaoyong, S.; Liangcheng, C.; Honglin, M.; Peng, G.; Zhanwei, B.; Cheng, L.: Experimental analysis of high temperature PEEK materials on 3D printing test. In: Proceedings—9th International Conference on Measuring Technology and Mechatronics Automation, ICMTMA 2017, pp. 13–16 (2017). <https://doi.org/10.1109/ICMTMA.2017.0012>
  24. Park, S.J.; Lee, J.E.; Park, J.; Lee, N.K.; Son, Y.; Park, S.H.: High-temperature 3D printing of polyetheretherketone products: Perspective on industrial manufacturing applications of super engineering plastics. *Mater. Des.* **211**, 110163 (2021). <https://doi.org/10.1016/j.matdes.2021.110163>
  25. Do Jung, H.; Jang, T.S.; Lee, J.E.; Park, S.J.; Son, Y.; Park, S.H.: Enhanced bioactivity of titanium-coated polyetheretherketone implants created by a high-temperature 3D printing process. *Biofabrication* (2019). <https://doi.org/10.1088/1758-5090/ab376b>
  26. Garcia-Leiner, M.; Streifel, B.; Başıgöl, C.; MacDonald, D.W.; Kurtz, S.M.: Characterization of polyaryletherketone (PAEK) filaments and printed parts produced by extrusion-based additive manufacturing. *Polym. Int.* **70**(8), 1128–1136 (2021). <https://doi.org/10.1002/pi.6231>
  27. Wu, W., et al.: 3D printing of thermoplastic PI and interlayer bonding evaluation. *Mater. Lett.* **229**, 206–209 (2018). <https://doi.org/10.1016/j.matlet.2018.07.020>
  28. El Magri, A.; Vanai, S.; Vaudreuil, S.: An overview on the influence of process parameters through the characteristic of 3D-printed PEEK and PEI parts. *High Perform. Polym.* **33**(8), 862–880 (2021). <https://doi.org/10.1177/09540083211009961>
  29. Afghah, F., et al.: 3D printing of silver-doped polycaprolactone-poly propylene succinate composite scaffolds for skin tissue engineering. *Biomed. Mater.* (2020). <https://doi.org/10.1088/1748-605X/ab7417>
  30. Park, S.J., et al.: 3D printing of bio-based polycarbonate and its potential applications in ecofriendly indoor manufacturing. *Addit. Manuf.* **31**, 100974 (2020). <https://doi.org/10.1016/j.addma.2019.100974>
  31. Patel, A.; Taufik, M.: Nanocomposite materials for fused filament fabrication. *Mater. Today Proc.* **47**, 5142–5150 (Jan.2021). <https://doi.org/10.1016/j.matpr.2021.05.438>
  32. Zaldivar, R.J.; Witkin, D.B.; McLouth, T.; Patel, D.N.; Schmitt, K.; Nokes, J.P.: Influence of processing and orientation print effects on the mechanical and thermal behavior of 3D-Printed ULTEM® 9085 Material. *Addit. Manuf.* **13**, 71–80 (2017). <https://doi.org/10.1016/j.addma.2016.11.007>
  33. Chacón, J.M.; Caminero, M.A.; Núñez, P.J.; García-Plaza, E.; García-Moreno, I.; Reverte, J.M.: Additive manufacturing of continuous fibre reinforced thermoplastic composites using fused deposition modelling: effect of process parameters on mechanical properties. *Compos. Sci. Technol.* **181**, 107688 (2019). <https://doi.org/10.1016/j.compscitech.2019.107688>
  34. Tran, T.Q.; Ng, F.L.; Kai, J.T.Y.; Feih, S.; Nai, M.L.S.: Tensile strength enhancement of fused filament fabrication printed parts: a review of process improvement approaches and respective impact. *Addit. Manuf.* **54**, 102724 (2022). <https://doi.org/10.1016/j.addma.2022.102724>
  35. Mackay, M.E.: The importance of rheological behavior in the additive manufacturing technique material extrusion. *J. Rheol. (N. Y. N. Y.)* **62**(6), 1549–1561 (2018). <https://doi.org/10.1122/1.5037687>
  36. van de Werken, N.; Tekinalp, H.; Khanbolouki, P.; Ozcan, S.; Williams, A.; Tehrani, M.: Additively manufactured carbon fiber-reinforced composites: state of the art and perspective. *Addit. Manuf.* **31**, 100962 (2020). <https://doi.org/10.1016/j.addma.2019.100962>
  37. Hu, C.; Qin, Q.H.: Advances in fused deposition modeling of discontinuous fiber/polymer composites. *Curr. Opin. Solid State Mater. Sci.* **24**(5), 100867 (2020). <https://doi.org/10.1016/j.cossms.2020.100867>
  38. Koch, C.; Van Hulle, L.; Rudolph, N.: Investigation of mechanical anisotropy of the fused filament fabrication process via customized tool path generation. *Addit. Manuf.* **16**, 138–145 (2017). <https://doi.org/10.1016/j.addma.2017.06.003>
  39. Alaimo, G.; Marconi, S.; Costato, L.; Auricchio, F.: Influence of meso-structure and chemical composition on FDM 3D-printed parts. *Compos. Part B Eng.* **113**, 371–380 (2017). <https://doi.org/10.1016/j.compositesb.2017.01.019>
  40. Rodriguez, J.F.; Thomas, J.P.; Renaud, J.E.: Characterization of the mesostructure of fused-deposition acrylonitrile-butadienestyrene materials. *Rapid Prototyp. J.* **6**(3), 175–185 (2000). <https://doi.org/10.1108/13552540010337056>
  41. Ang, K.C.; Leong, K.F.; Chua, C.K.; Chandrasekaran, M.: Investigation of the mechanical properties and porosity relationships in fused deposition modelling-fabricated porous structures. *Rapid Prototyp. J.* **12**(2), 100–105 (2006). <https://doi.org/10.1108/13552540610652447>
  42. Xiao, X.; Chevali, V.S.; Song, P.; He, D.; Wang, H.: Polylactide/hemp hurd biocomposites as sustainable 3D printing feedstock. *Compos. Sci. Technol.* **184**, 107887 (2019). <https://doi.org/10.1016/j.compscitech.2019.107887>
  43. Kio, O.J., et al.: Non-destructive evaluation of additively manufactured polymer objects using X-ray interferometry. *Addit. Manuf.* **24**, 364–372 (2018). <https://doi.org/10.1016/j.addma.2018.04.014>
  44. Penumakala, P.K.; Santo, J.; Thomas, A.: A critical review on the fused deposition modeling of thermoplastic polymer composites. *Compos. Part B Eng.* **201**, 108336 (2020). <https://doi.org/10.1016/j.compositesb.2020.108336>
  45. Wu, H., et al.: Recent developments in polymers/polymer nanocomposites for additive manufacturing. *Prog. Mater. Sci.* (2020). <https://doi.org/10.1016/j.pmatsci.2020.100638>
  46. Alsoufi, M.S.; Elsayed, A.E.: Warping deformation of desktop 3D printed parts manufactured by open source fused deposition modeling (FDM) system. *Int. J. Mech. Mechatron. Eng.* **17**(4), 7–16 (2017)
  47. Akhouni, B.; Behraves, A.H.: Effect of filling pattern on the tensile and flexural mechanical properties of FDM 3D printed products. *Exp. Mech.* **59**(6), 883–897 (2019). <https://doi.org/10.1007/s11340-018-00467-y>
  48. Jabbari, A.; Abrinia, K.: Developing thixo-extrusion process for additive manufacturing of metals in semi-solid state. *J. Manuf. Process.* **35**, 664–671 (2018). <https://doi.org/10.1016/j.jmapro.2018.08.031>
  49. Sukindar, N.A.; Ariffin, M.K.A.M.; Baharudin, B.T.H.T.; Jaafar, C.N.A.; Ismail, M.I.S.: Effects of nozzle die angle on extruding polymethylmethacrylate in open-source 3D printing. *J. Comput. Theor. Nanosci.* **15**(2), 663–665 (2018). <https://doi.org/10.1166/jctn.2018.7141>
  50. Ahn, S.H.; Montero, M.; Odell, D.; Roundy, S.; Wright, P.K.: Anisotropic material properties of fused deposition modeling ABS. *Rapid Prototyp. J.* **8**(4), 248–257 (2002). <https://doi.org/10.1108/13552540210441166>
  51. Lalegani Dezaki, M.; Mohd Ariffin, M.K.A.; Hatami, S.: An overview of fused deposition modelling (FDM): research, development and process optimisation. *Rapid Prototyp. J.* **27**(3), 562–582 (2021). <https://doi.org/10.1108/RPJ-08-2019-0230>

52. Yang, L.; Li, S.; Li, Y.; Yang, M.; Yuan, Q.: Experimental investigations for optimizing the extrusion parameters on FDM PLA printed parts. *J. Mater. Eng. Perform.* **28**(1), 169–182 (2019). <https://doi.org/10.1007/s11665-018-3784-x>
53. Mireles, J.; Espalin, D.; Roberson, D.; Zinniel, B.; Medina, F.; Wicker, R.: Fused deposition modeling of metals. In: 2022 Annual International Solid Freeform Fabrication Symposium an Additive Manufacturing Conference SFF 2012, pp. 836–845 (2012).
54. Coogan, T.J.; Kazmer, D.O.: In-line rheological monitoring of fused deposition modelling. *J. Rheol. (N. Y. N. Y.)* **63**(1), 141–155 (2019). <https://doi.org/10.1122/1.5054648>
55. Kazmer, D.O.: Injection mold design engineering. *Inject. Mold Des. Eng.* (2007). <https://doi.org/10.3139/9783446434196>
56. Gogos, C.G.; Tadmor, Z.: Principles of Polymer Processing. Wiley, New York (2013)
57. Wool, R.P.; Yuan, B.-L.; McGarel, O.J.: Welding of polymer interfaces. *Polym. Eng. Sci.* **29**(19), 1340–1367 (1989). <https://doi.org/10.1002/pen.760291906>
58. Yang, Z.; Jin, L.; Yan, Y.; Mei, Y.: Filament breakage monitoring in fused deposition modeling using acoustic emission technique. *Sensors (Switz.)* **18**(3), 1–16 (2018). <https://doi.org/10.3390/s18030749>
59. Agarwala, M.K.; Jamalabad, V.R.; Langrana, N.A.; Safari, A.; Whalen, P.J.; Danforth, S.C.: Structural quality of parts processed by fused deposition. *Rapid Prototyp. J.* (1996). <https://doi.org/10.1108/13552549610732034>
60. Bellini, A.; Güçeri, S.; Bertoldi, M.: Liquefier dynamics in fused deposition. *J. Manuf. Sci. Eng. Trans. ASME* **126**(2), 237–246 (2004). <https://doi.org/10.1115/1.1688377>
61. Crockett, R.S.; Calvert, P.D.: In: Stereodeposition techniques. *Process. 1996 Int. Solid Free. Fabr. Symp.*, pp. 257–264 (1996).
62. Venkataraman, N., et al.: Feedstock material property—process relationships in fused deposition of ceramics (FDC). *Rapid Prototyp. J.* **6**(4), 244–252 (2000). <https://doi.org/10.1108/13552540010373344>
63. Rao, P.K.; Liu, J.; Roberson, D.; Kong, Z.; Williams, C.: Online real-time quality monitoring in additive manufacturing processes using heterogeneous sensors. *J. Manuf. Sci. Eng. Trans. ASME* (2015). <https://doi.org/10.1115/1.4029823>
64. Gibson, M.A., et al.: 3D printing metals like thermoplastics: fused filament fabrication of metallic glasses. *Mater. Today* **21**(7), 697–702 (2018). <https://doi.org/10.1016/j.mattod.2018.07.001>
65. Ashby, M.F.; Greer, A.L.: Metallic glasses as structural materials. *Scr. Mater.* **54**(3), 321–326 (2006). <https://doi.org/10.1016/j.scriptamat.2005.09.051>
66. Lewandowski, J.J.; Wang, W.H.; Greer, A.L.: Intrinsic plasticity or brittleness of metallic glasses. *Philos. Mag. Lett.* **85**(2), 77–87 (2005). <https://doi.org/10.1080/09500830500080474>
67. Pang, S.J.; Zhang, T.; Asami, K.; Inoue, A.: Synthesis of Fe–Cr–Mo–C–B–P bulk metallic glasses with high corrosion resistance. *Acta Mater.* **50**(3), 489–497 (2002). [https://doi.org/10.1016/S1359-6454\(01\)00366-4](https://doi.org/10.1016/S1359-6454(01)00366-4)
68. Waniuk, T.; Schroers, J.; Johnson, W.L.: Timescales of crystallization and viscous flow of the bulk glass-forming Zr–Ti–Ni–Cu–Be alloys. *Phys. Rev. B Condens. Matter. Mater. Phys.* **67**(18), 1–9 (2003). <https://doi.org/10.1103/PhysRevB.67.184203>
69. Zhang, C.; Wang, W.; Li, Y.C.; Yang, Y.G.; Wu, Y.; Liu, L.: 3D printing of Fe-based bulk metallic glasses and composites with large dimensions and enhanced toughness by thermal spraying. *J. Mater. Chem. A* **6**(16), 6800–6805 (2018). <https://doi.org/10.1039/c8ta00405f>
70. Bordeenithakasem, P.; Stolpe, M.; Elsen, A.; Hofmann, D.C.: Glass forming ability, flexural strength, and wear properties of additively manufactured Zr-based bulk metallic glasses produced through laser powder bed fusion. *Addit. Manuf.* **21**(2010), 312–317 (2018). <https://doi.org/10.1016/j.addma.2018.03.023>
71. Ouyang, D.; Li, N.; Xing, W.; Zhang, J.; Liu, L.: 3D printing of crack-free high strength Zr-based bulk metallic glass composite by selective laser melting. *Intermetallics* **90**, 128–134 (2017). <https://doi.org/10.1016/j.intermet.2017.07.010>
72. Tlegenov, Y.; Hong, G.S.; Lu, W.F.: Nozzle condition monitoring in 3D printing. *Robot. Comput. Integr. Manuf.* **54**, 45–55 (2018). <https://doi.org/10.1016/j.rcim.2018.05.010>
73. Loke, G., et al.: Structured multimaterial filaments for 3D printing of optoelectronics. *Nat. Commun.* (2019). <https://doi.org/10.1038/s41467-019-11986-0>
74. Rafiee, M.; Farahani, R.D.; Therriault, D.: Multi-material 3D and 4D printing: a survey. *Adv. Sci.* **7**(12), 1–26 (2020). <https://doi.org/10.1002/advs.201902307>
75. Han, S.; Xiao, Y.; Qi, T.; Li, Z.; Zeng, Q.: Design and analysis of fused deposition modeling 3D printer nozzle for color mixing. *Adv. Mater. Sci. Eng.* (2017). <https://doi.org/10.1155/2017/2095137>
76. Abilgazyev, A.; Kulzhan, T.; Raissov, N.; Ali, M.H.; Match, W.L.K.O.; Mir-Nasiri, N.: Design and development of multi-nozzle extrusion system for 3D printer. In: 2015 4th International Conference on Informatics, Electronics, Vision, ICIEV 2015 (2015). <https://doi.org/10.1109/ICIEV.2015.7333982>
77. Ali, M.H.; Mir-Nasiri, N.; Ko, W.L.: Multi-nozzle extrusion system for 3D printer and its control mechanism. *Int. J. Adv. Manuf. Technol.* **86**(1–4), 999–1010 (2016). <https://doi.org/10.1007/s00170-015-8205-9>
78. Lopes, L.R.; Silva, A.F.; Carneiro, O.S.: Multi-material 3D printing: the relevance of materials affinity on the boundary interface performance. *Addit. Manuf.* **23**, 45–52 (2018). <https://doi.org/10.1016/j.addma.2018.06.027>
79. Waly, C.; Petersmann, S.; Arbeiter, F.: Multimaterial extrusion-based additive manufacturing of compliant crack arrester: influence of interlayer length, thickness, and applied strain rate. *Adv. Eng. Mater.* (2022). <https://doi.org/10.1002/adem.202101703>
80. Ahmed, S.W., et al.: On the effects of process parameters and optimization of interlaminar bond strength in 3D printed ABS/CF-PLA composite. *Polymers (Basel)*. (2020). <https://doi.org/10.3390/POLYM12092155>
81. Quero, R.F.; de Costa, B.M.C.; da Silva, J.A.F.; de Jesus, D.P.: Using multi-material fused deposition modeling (FDM) for one-step 3D printing of microfluidic capillary electrophoresis with integrated electrodes for capacitively coupled contactless conductivity detection. *Sensors Actuators B Chem.* (2022). <https://doi.org/10.1016/j.snb.2022.131959>
82. Wang, W., et al.: Enhancing the hydrophilicity and cell attachment of 3D printed PCL/graphene scaffolds for bone tissue engineering. *Materials (Basel)*. (2016). <https://doi.org/10.3390/ma9120992>
83. Geoffroy, L.; Samyn, F.; Jimenez, M.; Bourbigot, S.: Additive manufacturing of fire-retardant ethylene-vinyl acetate. *Polym. Adv. Technol.* **30**(7), 1878–1890 (2019). <https://doi.org/10.1002/pat.4620>
84. Goyanes, A.; Allahham, N.; Trenfield, S.J.; Stoyanov, E.; Gaisford, S.; Basit, A.W.: Direct powder extrusion 3D printing: fabrication of drug products using a novel single-step process. *Int. J. Pharm.* (2019). <https://doi.org/10.1016/j.ijpharm.2019.118471>
85. Lengauer, W.; et al.: Preparation and properties of extrusion-based 3D-printed hardmetal and cermet parts. In: Euro PM2018 Congress & Exhibition (2020).
86. Woern, A.L.; Byard, D.J.; Oakley, R.B.; Fiedler, M.J.; Snabes, S.L.; Pearce, J.M.: Fused particle fabrication 3-D printing: recycled materials’ optimization and mechanical properties. *Materials (Basel)* (2018). <https://doi.org/10.3390/ma11081413>
87. Moreno Nieto, D.; Casal López, V.; Molina, S.I.: Large-format polymeric pellet-based additive manufacturing for the naval industry. *Addit. Manuf.* **23**, 79–85 (2018). <https://doi.org/10.1016/j.addma.2018.07.012>



88. Kumar, N.; Jain, P.K.; Tandon, P.; Pandey, P.M.: Extrusion-based additive manufacturing process for producing flexible parts. *J. Braz. Soc. Mech. Sci.* **40**(3), 1–12 (2018). <https://doi.org/10.1007/s40430-018-1068-x>
89. Bellini, A.: Fused deposition modelling of ceramics: A comprehensive experimental, analytical and computational study of material behaviour, fabrication process and equipment design. Dissertation, Drexel University (2002)
90. Bellini, A.; Shor, L.; Guceri, S.I.: New developments in fused deposition modeling of ceramics. *Rapid Prototyp. J.* (2005). <https://doi.org/10.1108/13552540510612901>
91. Wang, F., et al.: Precision extruding deposition and characterization of cellular poly- $\epsilon$ -caprolactone tissue scaffolds. *Rapid Prototyp. J.* **10**(1), 42–49 (2004). <https://doi.org/10.1108/13552540410512525>
92. de Silveira, Z.C.; de Freitas, M.S.; Neto, P.I.; Noritomi, P.Y.; da Silva, J.V.L.: Design development and functional validation of an interchangeable head based on mini screw extrusion applied in an experimental desktop 3-D printer. *Int. J. Rapid Manuf.* **4**(1), 49 (2014). <https://doi.org/10.1504/ijrapidm.2014.062037>
93. Tseng, J.W., et al.: Screw extrusion-based additive manufacturing of PEEK. *Mater. Des.* **140**, 209–221 (2018). <https://doi.org/10.1016/j.matdes.2017.11.032>
94. Zhou, Z.; Salaoru, I.; Morris, P.; Gibbons, G.J.: Additive manufacturing of heat-sensitive polymer melt using a pellet-fed material extrusion. *Addit. Manuf.* **24**, 552–559 (2018). <https://doi.org/10.1016/j.addma.2018.10.040>
95. Leng, J.; Wu, J.; Chen, N.; Xu, X.; Zhang, J.: The development of a conical screw-based extrusion deposition system and its application in fused deposition modeling with thermoplastic polyurethane. *Rapid Prototyp. J.* **26**(2), 409–417 (2020). <https://doi.org/10.1108/RPJ-05-2019-0139>
96. Annoni, M.; Giberti, H.; Strano, M.: Feasibility study of an extrusion-based direct metal additive manufacturing technique. *Procedia Manuf.* **5**, 916–927 (2016). <https://doi.org/10.1016/j.promfg.2016.08.079>
97. Canessa, E.; Baruzzo, M.; Fonda, C.: Study of Moineau-based pumps for the volumetric extrusion of pellets. *Addit. Manuf.* **17**, 143–150 (2017). <https://doi.org/10.1016/j.addma.2017.08.015>
98. Khondoker, M.A.H.; Sameoto, D.: Direct coupling of fixed screw extruders using flexible heated hoses for FDM printing of extremely soft thermoplastic elastomers. *Prog. Addit. Manuf.* **4**(3), 197–209 (2019). <https://doi.org/10.1007/s40964-019-00088-4>
99. Whyman, S.; Arif, K.M.; Potgieter, J.: Design and development of an extrusion system for 3D printing biopolymer pellets. *Int. J. Adv. Manuf. Technol.* **96**(9–12), 3417–3428 (2018). <https://doi.org/10.1007/s00170-018-1843-y>
100. Mudalamanan, R.; Bigio, D.I.: Process variations and the transient behavior of extruders. *AIChE J.* **49**(12), 3150–3160 (2003). <https://doi.org/10.1002/aic.690491215>
101. Drotman, D.; Arbor, A.; Bitmead, R.: Control-oriented energy-based modeling of a screw extruder used for 3D printing. In: ASME 2016 Dynamic Systems and Control Conference. American Society of Mechanical Engineers Digital Collection, pp. 1–7 (2016).
102. Albu, S.C.: Development on the production of a new type of extruder used in additive manufacturing, FDM technology. *Procedia Manuf.* **22**, 141–146 (2018). <https://doi.org/10.1016/j.promfg.2018.03.022>
103. Wankhade, M.H.; Bahale, S.G.: Design and development of plastic filament extruder for 3D printing. *IRA-Int. J. Technol. Eng.* **10**(3), 23 (2018). <https://doi.org/10.21013/jte.v10.n3.pl>
104. Krishnanand, V.; Singh, V.; Mittal, V.; Branwal, A.K.; Taufik, M.: Extruder Design in Pellets Operated 3D Printers: A Review, p. 661–675. Springer, Cham (2022)
105. Curmi, A.; Rochman, A.: From theory to practice: development and calibration of micro pellet extruder for additive manufacturing. *Key Eng. Mater.* **926**, 34–45 (2022). <https://doi.org/10.4028/p-b22a9a>
106. Krishnanand; Taufik, M.: Design and development of pellets/granules extrusion system for additive manufacturing. (2021). <https://doi.org/10.1115/IMECE2021-71083>
107. Albu, S.C.; Nuțiu, E.: Study on designing the extruder for 3D printers with pellets. *Acta Marisiensis. Ser. Technol.* **16**(1), 19–22 (2019). <https://doi.org/10.2478/amset-2019-0004>
108. Krishnanand, A.; Soni, S.; Nayak, A.; Taufik, M.: Development of graphics user interface (GUI) for process planning in extrusion based additive manufacturing. *Mater. Today Proc.* (2021). <https://doi.org/10.1016/j.matpr.2021.02.306>
109. Kumar, S.; Singh, R.; Singh, T.P.; Batish, A.: On twin screw extrusion parametric optimisation using hybrid approach of ANOVA and TOPSIS for 3D printing applications. *Adv. Mater. Process. Technol.* (2022). <https://doi.org/10.1080/2374068X.2022.2087844>
110. Hertle, S.; Drexler, M.; Drummer, D.: Additive manufacturing of poly(propylene) by means of melt extrusion. *Macromol. Mater. Eng.* **301**(12), 1482–1493 (2016). <https://doi.org/10.1002/mame.201600259>
111. Magnoni, P.; Rebaioli, L.; Fassi, I.; Pedrocchi, N.; Tosatti, L.M.: Robotic AM system for plastic materials: tuning and on-line adjustment of process parameters. *Procedia Manuf.* **11**, 346–354 (2017). <https://doi.org/10.1016/j.promfg.2017.07.117>
112. Brooks, B.J.; Arif, K.M.; Dirven, S.; Potgieter, J.: Robot-assisted 3D printing of biopolymer thin shells. *Int. J. Adv. Manuf. Technol.* **89**(1–4), 957–968 (2017). <https://doi.org/10.1007/s00170-016-9134-y>
113. Liu, X.; Chi, B.; Jiao, Z.; Tan, J.; Liu, F.; Yang, W.: A large-scale double-stage-screw 3D printer for fused deposition of plastic pellets. *J. Appl. Polym. Sci.* **134**(31), 1–9 (2017). <https://doi.org/10.1002/app.45147>
114. Duty, C.E., et al.: Structure and mechanical behavior of big area additive manufacturing (BAAM) materials. *Rapid Prototyp. J.* **23**(1), 181–189 (2017). <https://doi.org/10.1108/RPJ-12-2015-0183>
115. Ramanath, H.S.; Chua, C.K.; Leong, K.F.; Shah, K.D.: Melt flow behaviour of poly- $\epsilon$ -caprolactone in fused deposition modelling. *J. Mater. Sci. Mater. Med.* **19**(7), 2541–2550 (Jul.2008). <https://doi.org/10.1007/s10856-007-3203-6>
116. Bin Sukindar, N.A.; Bin Mohd Ariffin, M.K.A.; Tuah Bin Baharudin, B.T.H.; Binti Jaafar, C.N.A.; Bin Ismail, M.I.S.: Analysis on temperature setting for extruding polylactic acid using open-source 3D printer. *ARPN J. Eng. Appl. Sci.* **12**(4), 1348–1353 (2017)
117. Khondoker, M.A.H.; Sameoto, D.: Design and characterization of a bi-material co-extruder for fused deposition modeling (2016) <https://doi.org/10.1115/imece2016-65330>
118. Kumar, N.; Jain, P.K.; Tandon, P.; Mohan Pandey, P.: Experimental investigations on suitability of polypropylene (PP) and ethylene vinyl acetate (EVA) in additive manufacturing. *Mater. Today Proc.* **5**(2), 4118–4127 (2018). <https://doi.org/10.1016/j.matpr.2017.11.672>
119. Kumar, N.; Jain, P.K.; Tandon, P.; Pandey, P.M.: The effect of process parameters on tensile behavior of 3D printed flexible parts of ethylene vinyl acetate (EVA). *J. Manuf. Process.* **35**, 317–326 (2017). <https://doi.org/10.1016/j.jmapro.2018.08.013>
120. Kumar, N.; Jain, P.K.; Tandon, P.; Pandey, P.M.: Investigation on the effects of process parameters in CNC assisted pellet based fused layer modeling process. *J. Manuf. Process.* **35**, 428–436 (2017). <https://doi.org/10.1016/j.jmapro.2018.08.029>

121. Kumar, N.; Jain, P.K.; Tandon, P.; Pandey, P.M.: Investigations on the melt flow behaviour of aluminium filled ABS polymer composite for the extrusion-based additive manufacturing process. *Int. J. Mater. Prod. Technol.* **59**(3), 194–211 (2019). <https://doi.org/10.1504/IJMPT.2019.102931>
122. Gawali, S.K.; Pandey, G.C.; Bajpai, A.; Jain, P.K.: Large-part manufacturing using CNC-assisted material extrusion-based additive manufacturing: issues and challenges. *Int. J. Interact. Des. Manuf.* (2022). <https://doi.org/10.1007/s12008-022-01097-4>
123. Alam, M.A.; Krishnanand; Patel, A.; Purohit, R.; Taufik, M.: Thermal analysis for improvement of mechanical properties in fused filament fabricated parts. *Int. J. Interact. Des. Manuf.* **1**, 2 (2022). <https://doi.org/10.1007/S12008-022-00981-3>
124. Rishi, O.: Feed rate effects in freeform filament extrusion feed rate effects in freeform filament extrusion (2013).
125. Drotman, D.T.J.: Design of a screw extruder for additive manufacturing, p. 57 (2015).

Springer Nature or its licensor (e.g. a society or other partner) holds exclusive rights to this article under a publishing agreement with the author(s) or other rightsholder(s); author self-archiving of the accepted manuscript version of this article is solely governed by the terms of such publishing agreement and applicable law.